Thesis for the Degree of Master of Science

Preparation and Characterization of nanoparticles/graphene oxide hybrid nanostructures

By

Pham Tuan Anh

Department of Image Science and Engineering

The Graduate School

Pukyong National University

August 2011

Preparation and Characterization of nanoparticles/graphene oxide hybrid nanostructures

(나노입자/산화 그래핀 혼성 나노구조의 제조 및 특성연구)

Advisor: Prof. Yeon Tae Jeong

By

Pham Tuan Anh

A thesis submitted in partial fulfillment of the requirements
for the degree of

Master of Science

In the Department of Image Science and Engineering, The Graduate School,
Pukyong National University

August 2011

Preparation and Characterization of nanoparticles/graphene oxide hybrid nanostructures

A dissertation

By

Pham Tuan Anh

Approved by:

Kwon Taek Lim, Ph.D. (Chairman)

Jong Su Kim, Ph.D. (Member)

Yeon Tae Jeong, Ph.D. (Member)

August 2011

Dedicated to My Loving Parents,

My sister

And

To whom I love...

ABSTRACT

The combination of carbon family materials such as, one dimensional (1D) carbon nanotubes (CNTs) and two dimensional (2D) graphene nanosheets with inorganic nanoparticles has opened up a new way to produce arrays of novel hybrid nanomaterials for various potential applications. As a novel carbon nanomaterial, graphene is expected as a high-potential nanoscale building block for developing such hybrid materials because it possesses large interfacial surface area as well as the superior electrical conductivity far much better than its analogous counterpart, CNTs. Along with relatively inexpensive sources (graphite) for preparing graphene, these advantages have led to the rise of scientific investigations among researchers in employing them as a cheap substitute for CNTs. In the frame of this thesis, new concepts for the functionalization of graphene based nanomaterials with various functional nanoparticles are presented. Up to date, although there were some reports on the immobilization of inorganic nanoparticles on graphene oxide, it is recognized that there is still a major drawback that must be overcome to meet requirements for practical applications. The drawback is that nanoparticles may easily leach out from the graphene surface during applications due to the weak interactions, such as electrostatic or π-π stacking interactions between graphene oxide surface and nanoparticles. The main goal in this thesis is to develop new and simple approaches for the immobilization of functional nanoparticles on graphene oxide surface by covalent bondings. The resulting hybrid nanostructures were characterized using a wide range of analytical techniques. The results underpinned in this thesis indicate that the potential of utilizing graphene-based hybrid nanostructure as a cost effective platform for many potential applications such as nanobiotechnology, solar energy conversion, photonic devices or catalysts.

LIST OF ABBREVIATIONS

AFM	Atomic force microscope
AuNPs	Gold nanoparticles
EDX	Energy dispersive X-ray analysis
FT-IR	Fourier transform infrared spectroscopy
GO	Graphene oxide
GONS	Graphene oxide nanosheets
GNS	Graphene nanosheets
^{1}H-NMR	^{1}H nuclear magnetic resonance
MNPs	Magnetic nanoparticles
PL	Photoluminescence
QDs	Quantum dots
FE-SEM	Field emission scanning electron microscope
SAED	Selected area electron diffraction pattern
SQUID	Superconducting quantum interference device magnetometer
TEM	Transmission electron microscope
TGA	Thermal gravimetric analyses
XPS	X-ray photoelectron spectroscopy
XRD	X-ray diffraction
UV-vis	Ultraviolet visible absorption spectra

ACKNOWLEDGEMENTS

There are many people to thank for their contributions, without which my Master studies at the Pukyong National University would have not been possible.

First of all, I am most grateful to my promoter, Prof. Dr. Yeon Tae Jeong, not only giving me the chance to work on the project, but also for general guidance, encouragement, and continuous support during my Master research.

Next, I would like to express my thanks to Dr. Aridoss and Dr. Ashok Kumar for their numerous fruitful discussions and critical reading and correcting of the manuscripts. I am also very grateful to my Korean Lab mates and my friends in the department, Min Sung Kim, Keun Soo Park, for helping me in various ways. I address my acknowledgements to the Brain Korea 21 program (BK21) for mainly financial support. Without this support, none of the research that presents in this thesis would have been accomplished. I would like to express my appreciation to the members of the Graduation Committee for their presents and comments on my work.

Before doing Master degree at the Pukyong National University, I had studied at the National Key for Polymer and Composites Materials at Hanoi University of Technology, Hanoi, Vietnam. I would like to thank Prof. Tran Vinh Dieu, who was my former supervisors during my early research at Hanoi University of Technology. I also express my deep gratitude to Prof. Quach Dinh Lien, for offering me a scientific position at Nha Trang University, Nha Trang, Vietnam after my graduation from Hanoi University of Technology.

Before finishing, I would like to thank my mom Nguyen Thi Mai, my father Pham Duy Quang, my sister Pham Hong Nhung and my girl friend Lam Minh Hoa for all their love and support. I thank you for encouraging me at every point of life and for standing besides me when I need a backing.

Contents

CHAPTER 1

Introduction

1.1. Introduction to chemical functionalization of graphene oxide

Graphene is an allotrope of carbon, whose structure is one-atom-think planar sheets of sp^2-bonded carbon atoms that are densely packed in a honeycomb crystal lattice. Since its discovery in 2004 [1], graphene has been emerging as a fascinating material because of its remarkable thermal, chemical, physical and electrical properties [2]. While these protocols have triggered burgeoning interest, the realization of these potential applications is limited due to difficulties in production individual graphene nanosheets. Hence, the development effective and scalable ways to prepare graphene is a great challenge for chemists. Currently, several methods to prepare graphene nanosheets have been developed, including chemical vapor deposition [3], chemical reduction [4], ultrasonic exfoliation [5], epitaxial growth [6]. Among these methods, the chemical reduction of graphene oxide (GO) using reducing agents is the most versatile and easily scalable method to produce graphene in a bulk quantity because it has advantage of an inexpensive way. Additionally, the presence of covalently attached oxygen-containing groups in graphene oxide (GO) such as hydroxyl; epoxy, carbonyl and carboxyl groups renders it strongly hydrophilic and also provides a handle for further surface chemical modifications via well developed carbon chemistry. Therefore, these stable flexible graphene oxide sheets are often used as the starting material for preparation of graphene-based hybrid materials. Up to date, a considerable number of studies have been reported on the field of chemistry functionalization of graphene oxide. In general, these methods could be divided into two categories: covalent

functionalization and non-covalent functionalization.

+ Covalent functionalization is based on the formation of covalent bonds between functional groups. A wide range of reactions using carboxylic group on graphene oxide surface to introduce small organic compounds, polymers or surfactants on its surface has been reported. These functionalization reactions often require activation of acid group using thionyl chloride or N,N'-dicyclohexylcarbodiimide. Subsequent addition of nucleophilic specices, such as amines or hydroxyls will introduce covalently functional groups to graphene oxide sheets via the formation of amidation reaction or esterification reaction. Introduction of substituted amines is one of the most commen methods of covalent functionalization of graphene oxide and this approach have been investigated for various applications in optoelectronic, biodevices or drug-delivery system. The covalent functionalization of graphene oxide with small organic compounds and polymers have been exploited to increase the dispersibility of chemically modified graphene sheets in both organic solvents and distilled water, thus making a flexibility of graphene for various potential applications.

+ The non-covalent functionalization is mainly used based on modification of graphene oxide with surfactants, small organic compounds, or polymers via adsorption forces such as Van der Waals force, hydrogen bonds, π-π stacking, electrostatic forces.

1.2. The development and application of nanoparticles/graphene hybrid materials

Recently, a new class of functional nanomaterials containing graphene and novel metal nanoparticles has been attracted a lot of interest in scientific communities due to these hybrid nanomaterials have many unique properties to meet various requirements for potential applications. The

dispersion of metal nanoparticles on graphene oxide surface sheets potentially provides an efficient way to optimize the optical, electrical, and catalytic properties of graphene sheets. The potential applications of graphene/nanoparticles hybrid are listed below:

- *Lithium Ion batteries:* Graphene is expected to be an advanced anode materials in Lithium Ion batteries due to its superior electrical conductivity, high surface to volume ratio, ultrathin thickness, structural flexibility. Recently, Wu and co-worker have reported a facile strategy to immobilize Co_3O_4 nanoparticles on graphene surface as an advanced anode materials for high performance Lithium Ion batteries [7].
- *Heterogeneous catalyst:* The combination of graphene sheets and novel nanoparticle offer an efficient way for catalysts of several chemical reactions. Because of inexpensive source and nontoxic properties, graphene is expected to provide a low-cost substitute for carbon nanotubes for heterogeneous catalyst with various functional nanoparticles. This was recently demonstrated by the immobilization of palladium nanoparticles and gold nanoparticles on graphene surface to obtain hybrid materials as active catalysts for the Suzuki reaction in aqueous media [8].
- *Biosensor:* Hybrid nanomaterials containing graphene and modified gold nanoparticles was used to fabricate biosensor for the determination of catechol. This biosensor exhibits high sensitivity, showing a great potential for rapid, cost-effective analysis of phenolic compounds [9].
- *Optoelectronic applications:* Considering ultrahigh electron conductivity and mobility, graphene should be a promising material to capture and transport electrons from excited quantum dots for optoelectronic applications. Recently, Quantum dots sensitized graphene provided a cost-

effective platform for solar energy conversion and other optoelectronic application [10].

1.3. Project description and objectives

The main goal of this work is to develop a new and simple approach for fabrication hybrid nanostrucdtures containing nanoparticles and graphene oxide via covalent functionalizations. Herein, we mainly focus on the immobilization of gold nanoparticles (AuNPs), CdS quantum dots (CdS QDs) and magnetic nanoparticles (MNPs) on the graphene sheets surface because these types of inorganic nanoparticles have many remarkable properties and potential applications. In this regard, the new three-step process has been developed, which includes: (1) functionalization of nanoparticles using small organic molecules via the well-developed thiol chemistry, (2) modification of graphene oxide to introduce functional groups on its surface, (3) the covalent immobilization of nanoparticles on graphene oxide surface via a simple chemical reaction.

1.4. Organization of this thesis

This thesis deals with the preparation of an array of novel hybrid nanomaterials containing graphene oxide and nanoparticles. I start by introduction the general concepts of chemistry functionalization of graphene for its applications in various fields of nanoscience and nanotechnology. Moreover, we also introduce the importance of graphene-nanoparticles hybrid materials for a wide range of potential applications and discuss the merits and demerits of the individual methods that were performed to prepare such hybrid materials. Individual chapters deal with immobilization of different types of nanoparticles onto the surface of graphene oxide to obtain novel hybrid nanostructures. In chapter 2, a novel hybrid material

containing graphene oxide, polymer and magnetic nanoparticle has been successful syntheiszed. The merit of this work is that mangetic nanoparticles were strongly immobilized onto the surface of graphene oxide via boroester bond. Moreover, the synthesized hybrid material has higly aqueous dispersions due to a due to a hydrophilic polymer, namely polyglycerol was covalently grafted to graphene oxide surface via *in situ* ring-opening polymerization of glycidol. In chapter 3 and chapter 4, I have developed a facile and efficient method to introduce gold nanoparticles and CdS quantum dots on graphene oxide surface via a simple amidation reaction. The results characterizations of the prepared hybrid nanostructures are discussed in detail in every chapter.

Bibliography

1. K.S. Novoselov, A.K. Geim, S.V. Morozov, D. Jiang, Y. Zhang, S.V. Dubonos, I.V. Grigorieva, A.A. Firsov, Science 306 (2004) 666.
2. J. Wu, W. Pisula, K. Mullen, Chem. Rew, 107 (2007) 718.
3. Reina, X. Jia, J. Ho, D. Nezich, H. Son, V. Bulovic, M.S. Dresselhaus and J. Kong, Nano Lett. 9 (2009) 30.
4. S. Stankovich, R. Piner, X. Chen, N. Wu, S.T. Nguyen and R.S. Ruoff, J. Mater. Chem. 16 (2006) 155.
5. M. Lotya, Y. Hernandez, P.J. King, R.J. Smith, V. Nicolosi, L.S. Karlsson, F.M. Blighe, S. De, Z. Wang, I.T. McGovern, G.S. Duesberg, and J.N. Coleman, J. Am. Chem. Soc. 131 (2009) 3611.
6. J. Park, W.C. Mitchel, L. Grazulis, H.E. Smith, K.G. Eyink, J.J. Boeckl, D.H. Tomich, S.D. Pacley, and J.E. Hoelscher, Adv. Mater. 22 (2010) 4140.
7. Z.S. Wu, W. Ren, L. Wen, L. Gao, J. Zhao, Z. Chen, G. Zhou, F. Li and

H.M. Cheng, ACS Nano 6 (2010) 3187.
8. Y. Li, X. Fan, J. Qi, J. Ji, S. Wang, G. Zhang, and F. Zhang, Nano Res, 6 (2010) 429.
9. W. Song, D.W. Li, Y.T. Li, Y. Li, Y.T. Longa, Biosens. Bioelectron, 26 (2011) 3181.
10. H. Chang, X. Lv, H. Zhang, J. Li Electron. Commun., 12 (2010) 483.

CHAPTER 2

Covalent functionalization of graphene oxide with polyglycerol and their use as templates for anchoring magnetic nanoparticles*

An efficient strategy for the preparation of water-dispersible hybrid material containing graphene oxide and polyglycerol for the first time is demonstrated. Pristine graphite was firstly oxidized to obtain graphene oxide with hydroxyl functional groups. Then, the covalent grafting of polyglycerol onto the surface of graphene oxide was carried out based on *in situ* ring-opening polymerization of glycidol. For the construction of novel hybrid nanostructure, Fe-core/Au-shell nanoparticles were prepared and further functionalized using 4-mercaptophenylboronic acid through the well-developed Au-S chemistry. Subsequently, magnetic nanoparticles were anchored on the surface of polyglycerol-grafted graphene nanosheets via boroester bonds. Fourier transform infrared spectroscopy was employed to investigate the initial changes in surface functionalities. While X-ray diffraction was used to confirm the structure of graphene oxide nanosheets, high resolution transmission electron microscopy and field emission scanning electronic microscopy equipped with an energy dispersive X-ray spectrometer were used to study the morphologies and distribution of magnetic nanoparticles onto the surface of polyglycerol-grafted graphene. Thermogravimetric analysis was used to study the weight loss of the samples on heating. Superconducting quantum interference device magnetometer was employed to the magnetic property of magnetic nanoparticles. The digital images provided a vivid observation on the high dispersion stability of the prepared novel hybrid materials in distilled water.

* This work was published in **Synthetic Metal, 2010, 160, 2028-2036.**

2.1. Introduction

The continuous progress of nanotechnology in material science has opened new pathways for developing of novel functional materials. Among them, graphene, a flat monolayer of hexagonally arrayed sp^2-bonded carbon atoms tightly packed into a two-dimensional (2D) honeycomb lattice, has been emerging as a fascinating material due to the unique physical, chemical, electrical and mechanical properties [1-6]. In parallel with developments from the basic science perspective [7-10], graphene-based hybrid materials with the combination of its excellent properties and inexpensive sources (from either natural or synthetic sources) have attracted a great deal of attention as promising candidates for a wide variety of potential applications in catalyst supports [11, 12], chemical sensors [13-16], electronic components [17-22], Li ion batteries [23, 24] and even applications in biotechnology [25, 26]. Among known studies for developing the graphene-based materials, utilization of graphene oxide (GO) is the most versatile and easily scalable [27]. Therefore, GO is often used as the starting material for the preparation of graphene-based hybrid materials. Although GO can be easily exfoliated into monolayer sheets in water, it is not quite ready for its potential applications due to the strong tendency of the monolayeric graphene sheet to form irreversible agglomerates into multilayeric graphite through strong π-π stacking and van der Waals interaction [28]. Therefore, the aggregation of graphene sheets poses a practical challenge, that must be addressed to expand graphene's application scope in various potential fields of nanotechnology because most of their unique properties are only associated with few layers or individual sheets of this two-dimensional hexagonally packed carbon lattice. It is well-known that the presence of covalently attached oxygen-containing groups in GO such as hydroxyl,

epoxy groups on the basal plane and carboxyl groups at the edge provides a handle for further surface chemical functionalizations via well-developed carbon chemistry. Hence, several chemical methods have been explored to obtain water-dispersible graphene that include noncovalent functionalization [29, 30] and covalent functionalization strategies [31-33].

Recently, a novel class of functional nanostructures has been developed to obtain the optical, electrical and catalytic properties via decorating graphene sheets with novel metal nanoparticles [34-36]. The dispersion of metal nanoparticles on graphene sheets provides new opportunities for researchers in designing novel hybrid nanostructures for various potential applications. It is well-known that many types of metals can be deposited onto surface of graphene sheets. Among such nanoparticles, magnetic nanoparticles have attracted a tremendous amount of attention in recent years due to their remarkable properties and potential applications [37-40]. However, reports on the immobilization of magnetic nanoparticles on the surface of GO sheets are relatively rare. Moreover, the lack of dispersibility of magnetic nanoparticles in solvents and the irreversible agglomerates of graphene have always been major technical barriers for the construction of hybrid nanostructures containing graphene and magnetic nanoparticles.

On the basis of these observations, in this contribution, we have explored a strategy for the covalent functionalization of graphene nanosheets with a class of hyperbranched polymers (aliphatic polyether polyols) named polyglycerol (PG) and their use as templates for further loading functionalized Fe-core/Au-shell nanoparticles (Fe@Au nanoparticles) for the first time. As a result, the combination of PG and GO leads to hybrid nanostructures with high dispersibility in aqueous media

mainly due to the high hydrophilicity of PG. Furthermore, the chemical grafting of PG onto the surface of GO also provides a suitable surface for their immobilization with functionalized magnetic nanoparticles to obtain novel nanostructures containing graphene, polymer and magnetic nanoparticles. To the best of our knowledge, there have been no reports available on using PG for the preparation of water-dispersible graphene hybrid nanostructures and their use as templates for loading Fe@Au nanoparticles.

In our strategy, GO was synthesized by the modified Hummer's and Offeman's method [41]. Subsequently, the chemical grafting of PG onto the GO sheets was carried out by the "grafting from" approach based on in-situ ring-opening polymerization of glycidol [42]. Furthermore, the Fe@Au nanoparticles were synthesized using the inverse micelle method [43]. To immobilize Fe@Au nanoparticles to the PG-grafted GO (PG-*g*-GO), the surface of Fe@Au nanoparticles was functionalized by boronic acid via the well-developed Au-S chemistry. The immobilization of boronic acid-modified magnetic nanoparticles on the PG-*g*-GO obtained through boroester bonds, which was formed between hydroxyl groups of boronic acid and PG. The combination of magnetic nanoparticles and biocompatible polymer, polyglycerol on to the GO sheets surface makes us believe that the novel hybrid materials developed in this study have potential for a wide variety of applications from electromagnetic devices to novel drug delivery systems.

2.2. Experimental sections

2.2.1. Materials

Graphite powder from Sigma-Aldrich was used to prepare GO.

Glycidol, potassium methoxide, 4-mercaptophenylboronic acid, ferrous sulfate, hydrogen tetrachloroaurate (gold solution; 30 wt.% in dilute HCl), sodium borohydride, cetyltrimethylammonium bromide, 1-butanol, octane and other chemicals were purchased from Sigma-Aldrich and used as received.

2.2.2. Preparation of GO

In a typical reaction, 3 g of graphite powder was added to 300 mL of cooled (0 °C) H_2SO_4. Then, 20 g of $KMnO_4$ and 3g of $NaNO_3$ were added slowly while stirring. The temperature of the mixture was maintained below 10 ^oC. The mixture was then transferred to a 35 °C water bath and stirred for 30 min. Subsequently, 200 mL of de-ionized water was added and the temperature was increased to 98^oC and the mixture was maintained at that temperature for 30min. The reaction was terminated by adding 500 mL of deionized water followed by the addition of 40 mL of 30% H_2O_2 solution. The color of the mixture changed to brilliant yellow, indicating the oxidation of pristine graphite to GO. The solid product was then separated by using membrane filter system, washed repeatedly with distilled water until the pH was 7 and dried at 50 ^oC for 24h under vacuum.

2.2.3. Synthesis of PG-*g*-GO

One hundred mg of GO was mixed with saturated solution of potassium methoxide in 2 mL of methanol for 1h in an ultrasonic bath and stirred at room temperature for 2h. Then, the mixture was refluxed at 80^oC for 6h and washed repeatedly with methanol. The solvent was removed by reduced pressure distillation in rotavapour. Then, 7 mL of glycidol was added to the GO and mixture was stirred for 4h at 100^oC under nitrogen atmosphere. The mixture was cooled and dissolved in methanol. Finally, the

product was precipitated in acetone and then separated by using membrane filter system.

2.2.4. Synthesis of boronic acid functionalized Fe@Au nanoparticles (B-*f*-MNPs)

Fe@Au nanoparticles were synthesized by a reverse micelle reaction under nitrogen atmosphere. All reverse micelle solutions were prepared using cetyltrimethylammonium (CTAB) as the surfactant, octane as the oil phase, 1-butanol as the cosurfactant, and aqueous reactant as the water phase. Firstly, 0.36 g of $FeSO_4$ in the inverse micelle solution was mixed up with 0.18 g of $NaBH_4$ in other reverse micelle solution. The mixture was stirred at room temperature under nitrogen atmosphere. The change in color of the solution from green to black, indicate the formation of Fe nanoparticles. After c.a. 1 h, 0.54 g of $HAuCl_4$ prepared as a micelle solution was added to the solution of $FeSO_4$ and $NaBH_4$. Then, 0.22 g of $NaBH_4$ in other micelle solution was immediately added to the solution. The new solution was left stirring at room temperature for 12 h under nitrogen atmosphere. The micelles in the reaction mixture were disrupted with acetone causing nanoparticles to precipitate. The dark solid was separated using a magnet and repeatedly washed with a 1:1 chloroform/methanol mixture to remove any nonmagnetic particles and organic surfactant if any. The product was then dried in vacuum oven for overnight, resulting in a black powder.

In the next step, 0.058 g of 4-mercaptophenylboronic acid was mixed with 0.03 g of Fe@Au nanoparticles in 50 mL of ethanol. After vigorous stirring for 12h, the solvent was removed by distillation under decreased pressure. The dark residue was washed thoroughly with diethyl ether to remove excess 4-mercaptophenylboronic acid. Finally, the material

was dried to obtain the pure product as a dark-brown solid.

2.2.5. Synthesis of magnetic nanoparticle-immobilized PG-*g*-GO (MNPs-*i*-PG-*g*-GO)

Twenty mg of PG-*g*-GO in 20 mL of ethanol were sonicated to obtain a homogeneous dispersion. Then the suspension of 0.01 g of B-*f*-MNPs in 10 mL of ethanol was added to the solution. The homogeneous black mixture was stirred at room temperature for 2h. The resultant black mixture was filtered, washed with ethanol and distilled water using PTFE filter membrane. The black solid was dried at 40^{o}C in a vacuum oven.

2.2.6. Characterization techniques

HR-TEM images were recorded using Joel JEM 2010 instrument (Japan) with an accelerating voltage of 200KV to observe the nanoscale structures, by placing a drop of the samples dispersed in distilled water on copper grids and drying. The morphology and elemental analysis of the hybrids were carried out by using FE-SEM images equipped with an EDX spectrometer (Hitachi JEOL-JSM-6700F system, Japan). The changes in the surface chemical bondings of functionalized Fe@Au nanoparticles and hybrid nanostructures were recorded by FT-IR (Perkin-Elmer Spectrum GX, USA), in the frequency range of 4000-500 cm^{-1}. Thermogravimetric analysis (TGA) was conducted with Perkin-Elmer Pyris 1 analyzer (USA). Before the test, all the samples were carefully grounded to fine powder. The samples were scanned within the temperature range 50-700^{o}C at a heating rate of 10^{o}C min^{-1} under continuous N_2 flow. Surface composition was investigated using X-ray photoelectron spectroscopy (Thermo VG Multilab 2000) in ultra high vacuum with Al *Kα*. The crystallographic states of Fe@Au nanoparticles, pristine graphite and hybrids were determined by a

Philips X'pert-MPD system diffractometer (Netherland) with Cu *Kα* radiation. Magnetic measurement was performed at 300K using a superconducting quantum interference device magnetometer (Quantum design MPMS-XL7, USA).

2.3. Results and discussion

2.3.1. Characterization of B-*f*-MNPs

Figure 1 shows HR-TEM images of Fe@Au nanoparticles. As seen from Figure 1a, it is interesting to note that the Fe@Au nanoparticles tend to aggregate into clusters, which is a result of the coating of Au layers to Fe nanoparticles. Clear observations on the core-shell structure of Fe@Au nanoparticles was obtained using the higher magnification HR-TEM as represented in Figure 1b. The size of Fe core is about 16 nm while the coating of Au shell is about 3~5 nm. The Fe core and Au shell are shown clearly marked arrows. In most of Fe@Au nanoparticles, shell of Au can be easily seen as bright regions in outer layer of nanoparticles, while the core of Fe appears as dark regions in the center of nanoparticles. It could be explained that Au, as a heavy element, scatters electrons more strongly than Fe with a smaller atomic number. Consequently, the brighter regions within the nanoparticles are Au rich, while the darker regions are Fe rich and Au poor [44]. The inset graph in Figure 1b shows diffraction studies of Fe@Au nanoparticle. The presence of both Au and Fe in a single particle was indicated through the overlapping of 200 and 220 of *fcc* structured Au with 110 and 200 of *bcc* structured Fe. In addition, the lattice fringes in the Au shells are clearly observed via high magnification HR-TEM image as seen in Figure 1c. Their inter-fringe spacing is 0.2 nm, indicating the interplane distance of the (200) planes of the *fcc* Au.

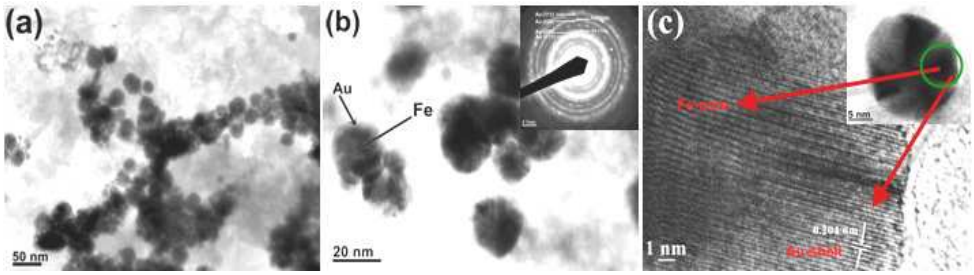

Figure 1. (a), (b) HR-TEM images of Fe@Au nanoparticles at different magnifications, the inset image shows diffraction pattern of a single Fe@Au nanoparticle and (c) HR-TEM image of a single Fe@Au nanoparticle.

More evidence, the crystalline structure of Fe@Au nanoparticles was obtained using XRD spectrum. As labeled in figure 2, the peaks at 38.14°, 44.36°, and 64.58° are assigned to *fcc* bulk Au of (111), (200), (220), (JCPDS 04-784). The pattern of Fe (JCPDS 06-696) is covered under the pattern of Au due to the overlapping of their diffraction peaks at 44.36° and 64.58°, indicating the presence of both Fe and Au nanoparticles in the sample.

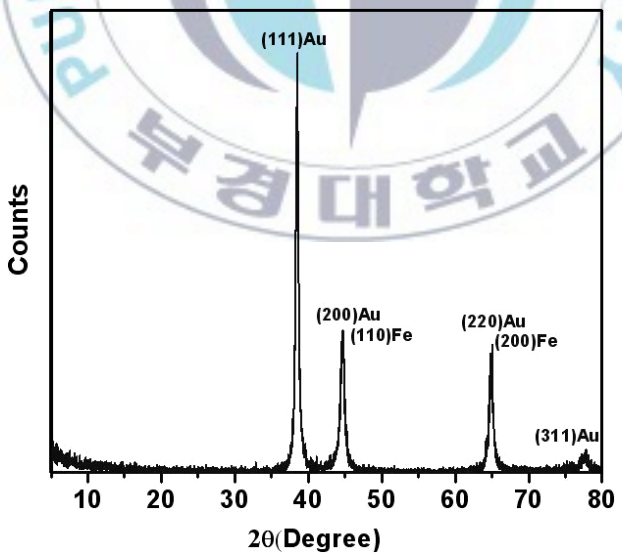

Figure 2. XRD pattern of Fe@Au nanoparticle.

The procedure for preparing of B-*f*-MNPs is presented in Scheme 1. To examine the surface functionalization of Fe@Au nanoparticles with boronic acid, FT-IR spectra of B-*f*-MNPs are shown in Figure 3a. The peaks at 3020 cm^{-1}, 1574 cm^{-1}, and 1013 cm^{-1} could be assigned to the presence of aromatic ring, while aryl-boroxines typically display at a band of 1368 cm^{-1} [45]. Furthermore, the board band at 3212 cm^{-1} indicates the presence of free hydroxyl functional groups of boronic acid on the sample surface. These results confirmed that surface of Fe@Au nanoparticles were successfully functionalized with 4-mercaptophenylboronic acid.

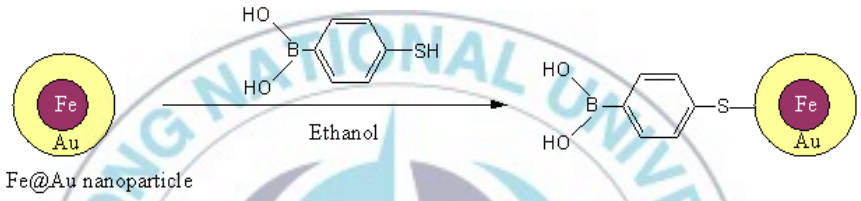

Scheme 1. Schematic illustration on the preparation of B-*f*-MNPs

On the other hand, to determine the magnetic property of synthesized B-*f*-MNPs, the magnetization measurement was carried out at room temperature. The saturation magnetization of the sample is 18 emu/g, indicating characteristic of superparamagnetic at room temperature presented in Figure 3b.

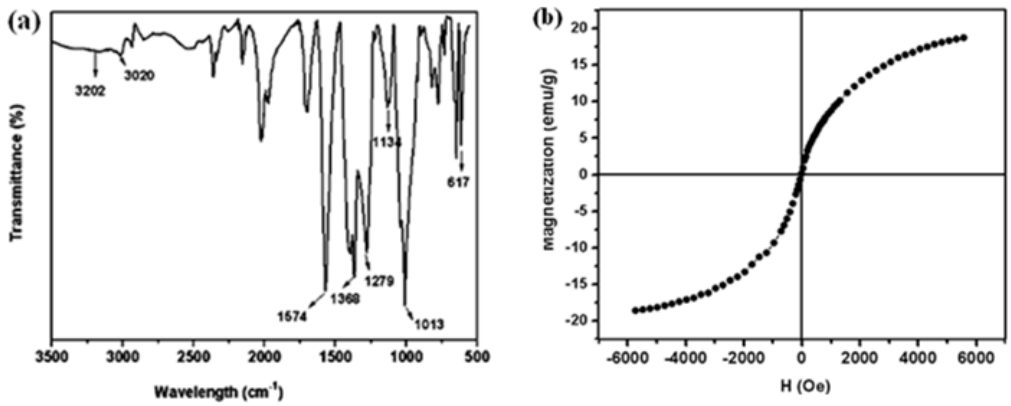

Figure 3. (a) FT-IR spectrum of B-*f*-MNPs and (b) magnetization curves of B-*f*-MNPs

2.3.2. Characterization of hybrid nanostructures

The schematic for preparing hybrid nanostructures is illustrated in Scheme 2. The three-step process includes: (1) the preparation of GO using Hummers and Offeman's method, (2) the chemical grafting of PG on the GO surface based on *in situ* ring-opening polymerization of glycidol and (3) the covalent immobilization of B-*f*-MNPs on the surface of PG-*g*-GO via boroester bonds.

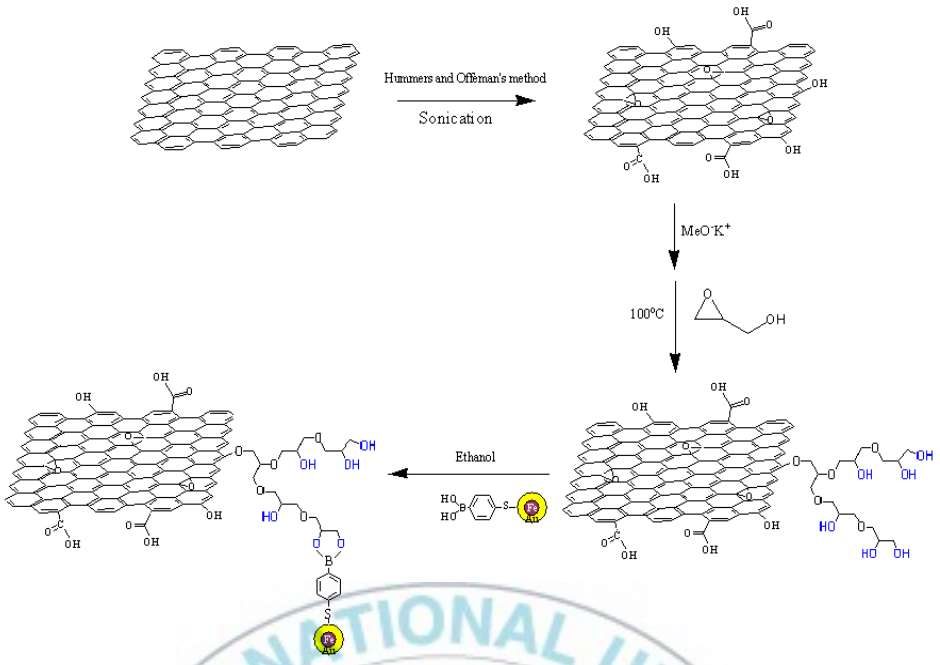

Scheme 2. Synthetic route of water-dispersible PG-*g*-GO nanostructure and its immobilization with the B-*f*-MNPs

Figure 4 shows the FT-IR results of the pristine graphite and hybrid nanostructures obtained at different processing step. For the pristine graphite, the peaks at 3016 and 1537 cm^{-1} are attributed to the presence of aromatic ring as shown in Figure 4a. The FI-IR spectrum of GO differs from that of pristine graphite as evidenced by the presence of new bands at 3188 and 1703 cm^{-1}. As can be seen from Figure 4b, the broad band at 3188 cm^{-1} could be assigned to stretching of the –OH groups on the GO surface, while the band at 1703 cm^{-1} is associated with stretching of the C=O bond of carboxylic groups. In the case of PG-*g*-GO, as seen in Figure 4c, the peaks at around 1711 and 1573 cm^{-1} continue to be observed in apart from the all features of the GO. However, the relative increase in the intensity of the broad band at around 3307 cm^{-1} suggests that there could be more –OH

groups on the surface of GO due to the presence of PG after the covalent grafting of PG to the GO surface. On the other hand, after the covalent immobilization of B-*f*-MNPs on the surface of PG-*g*-GO, significant changes were observed in the IR spectrum as shown in Figure 4d. New peaks at 1339 cm^{-1} and 616 cm^{-1} are assigned to B-O stretching band and B-O banding band, respectively and are clearly visible [46]. Moreover, the decrease in the intensity of the broad band around 3347 cm^{-1} was observed, indicating the density of hydroxyl groups on the PG-g-GO surface decreased after their reaction with boronic acid. These observations clearly confirmed the covalent immobilization of B-*f*-MNPs on the surface of PG-*g*-GO via boroester bonds.

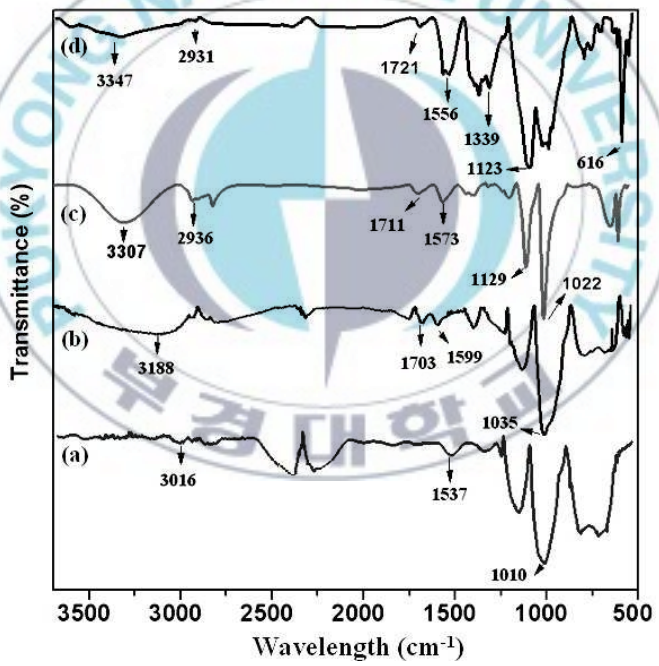

Figure 4. FT-IR spectra of (a) pristine graphite, (b) GO, (c) PG-*g*-GO and (d) MNPs-*i*-PG-*g*-GO.

To study the weight loss patterns of the synthesized hybrid nanostructures, TGA curves of the samples were scrutinized and are shown in Figure 5. As seen from Figure 5a, TGA traces of pristine graphite shows a negligible weight loss, which is about 2% of its total weight in the entire temperature range. Comparing with the pristine graphite, GO shows much lower thermal stability. Although there is a weight loss about 2% below 100^{o}C due to the removal of physically adsorbed water, the major weight loss occurs at 180^{o}C. As shown in Figure 5b, GO lose up to 98% of its total weight, which can be assigned to the pyrolysis of the labile oxygen-containing functional groups, yielding CO, CO_2 and steam [47]. On the other hand, the PG-*g*-GO and MNPs-*i*-PG-*g*-GO are more stable than GO as shown in Figure 5c and 5d. For both the samples, the main weight loss occurred around 300-400^{o}C. The increased thermal stability of the hybrid nanostructures could be attributed to the chemical grafting of PG onto the GO surface. It is worthy to note that, in the case of MNPs-*i*-PG-*g*-GO hybrid nanostructure, besides the presence of PG via chemical grafting, the binding of B-*f*-MNPs on the PG-*g*-GO surface also contribute to the increase in their thermal stability. The decomposition curve of pure PG is given in Figure 5e, which show a weight loss about 90% of its total weight which is in conjunction with previously reported study [48]. This also well suggests that the thermal stability of hybrid materials was better improved.

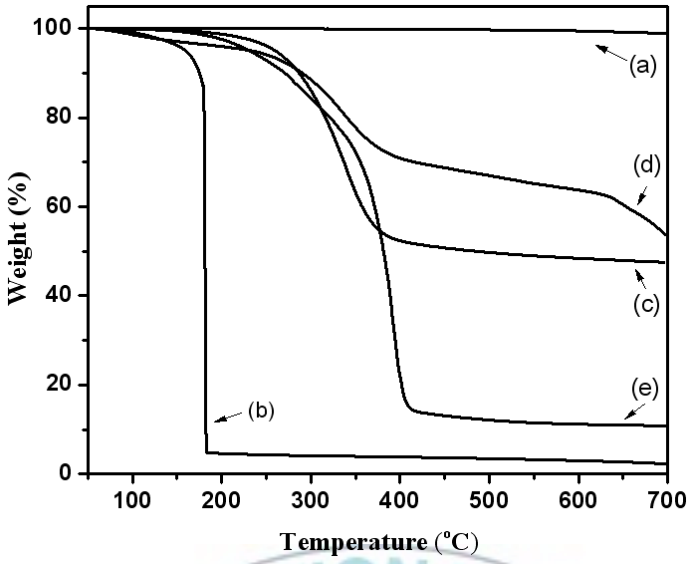

Figure 5. TGA curves of (a) pristine graphite, (b) GO, (c) PG-*g*-GO, (d) MNPs-*i*-PG-*g*-GO, and (e) pure PG.

XRD measurements were employed to investigate the crystallinity of the synthesized hybrids. Figure 6 depicts the XRD patterns of pristine graphite, GO and MNPs-*i*-PG-*g*-GO. While the characteristic peak corresponding to the (002) plane of pristine graphite appears at $2\theta = 26.67^{o}$, the GO pattern shows a strong peak at $2\theta = 11.7^{o}$, indicating the presence of oxygen-containing functional groups after the oxidation process as shown in Figure 6b. The d-spacing of GO layers calculated as 0.43 nm is larger than that of the layers of pristine graphite (0.25nm) [49]. As to the MNPs-*i*-PG-*g*-GO, after PG was grafted onto GO, the strong peak at 11.7^{o} disappeared, indicating the PG was successfully grafted on the GO surface. In addition, the pattern of MNPs-*i*-PG-*g*-GO shows four additional weak diffraction peaks at $2\theta = 38.14^{o}$, 44.36^{o}, 64.58^{o} and 77.8^{o}, which corresponds to the presence of Au and Fe nanoparticles on the surface of the samples (Figure 6c). The results demonstrate that the Fe@Au nanoparticles were

successfully immobilized onto the surface of PG-*g*-GO.

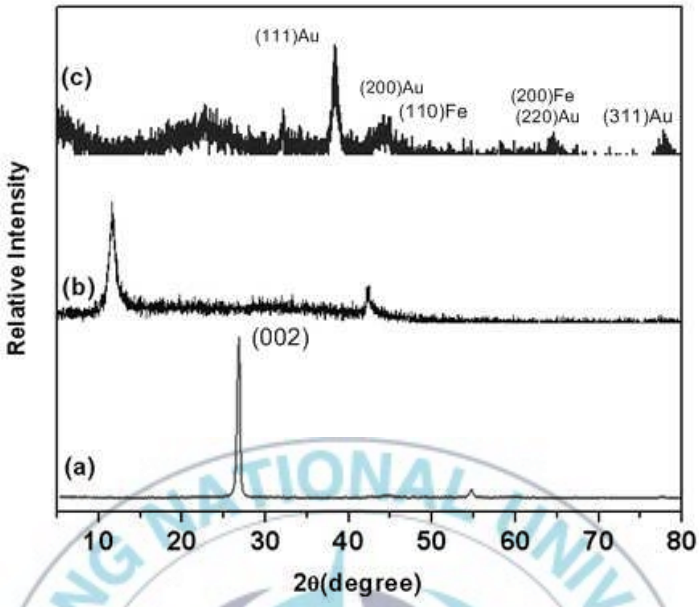

Figure 6. XRD pattern of (a) pristine graphite, (b) GO and (c) MNPs-*i*-PG-*g*-GO.

EDX analysis was also used to characterize the chemical composition of MNPs-*i*-PG-*g*-GO (Figure 7). The spectrum clearly shows the presence of gold, iron, sulfur, carbon and oxygen elements in the sample, which further confirm successful preparation of the novel hybrid nanostructures.

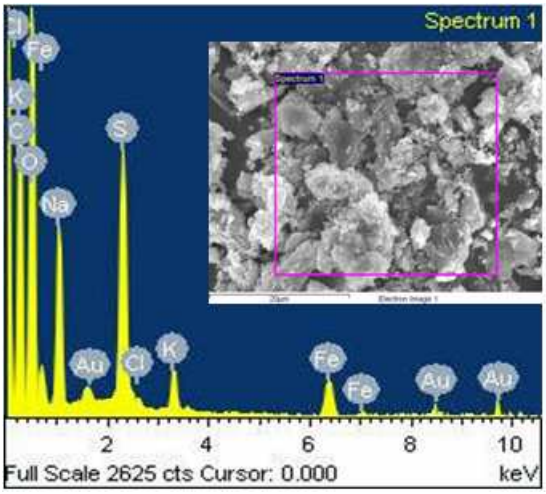

Figure 7. EDX spectrum of MNPs-*i*-PG-*g*-GO.

2.3.3. Morphologies of hybrid nanostructures

The morphologies of pristine graphite and the hybrid nanostructures were studied using FE-SEM as shown in Figure 8. Pristine graphite shows a laminated structure in which a large amount of sheets are stacked together (Figure 8a). In the case of GO, because of oxidation process, the GO sheets break into pieces smaller than pristine graphite which was observed in Figure 8b. On the other hand, as can be seen in Figure 8c and 8d, the PG-*g*-GO sample clearly reveals the thickness increase of these sheets when compared to the layered structures of GO (marked by arrows). This morphological observation indicates the surface of GO was grafted with PG. The morphology of the MNP-*i*-PG-*g*-GO represented in Figure 8e, clearly shows that the nanoparticle cluster was immobilized onto the PG-*g*-GO surface, hence indicating that there was strong interaction between PG-*g*-GO and B-*f*-MNPs via boroester bonds, which were formed between free hydroxyl functional groups present in PG and boronic acid.

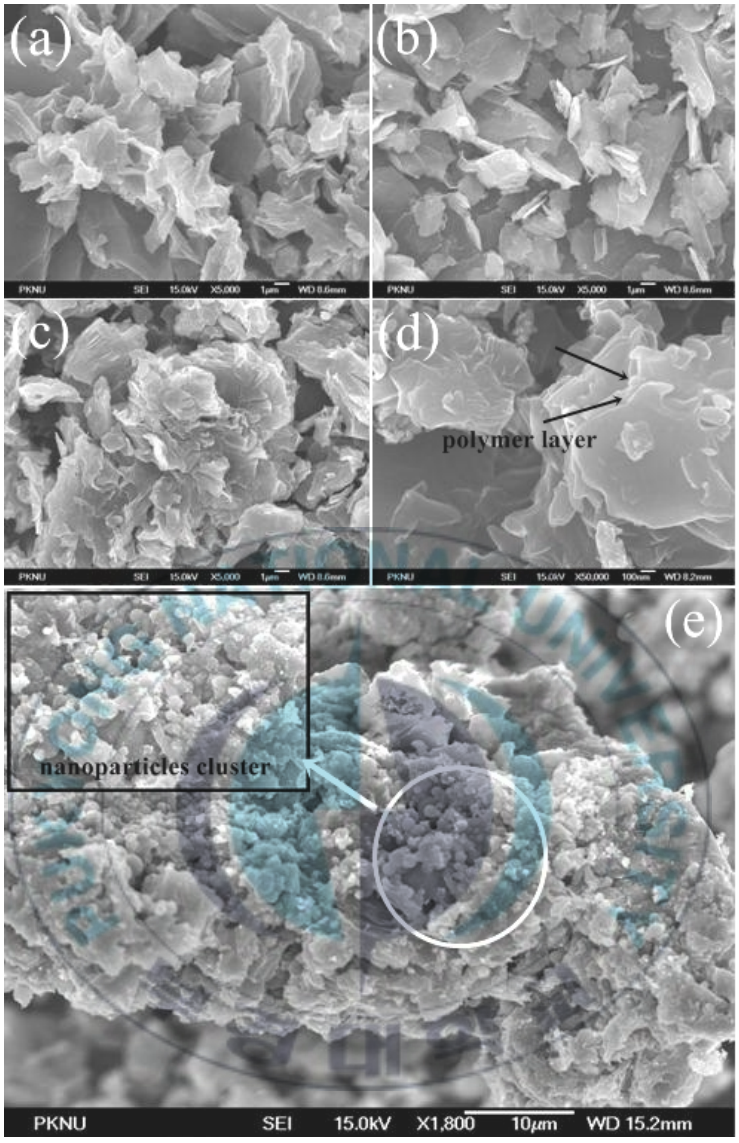

Figure 8. FE-SEM images of (a) pristine graphite, (b) GO, (c, d) PG-*g*-GO and (e) MNPs-*i*-PG-*g*-GO.

In order to further investigate the morphologies of the prepared hybrids, HR-TEM images were recorded. Figure 9 shows the TEM images of GO sheet, PG-*g*-GP and MNPs-*i*-PG-g-GO at different magnifications.

From the TEM images of GO, it can be seen the presence of a mixture of graphene layers. In most cases, bilayer graphene and few layers graphene were observed (Figure 9a). They are rippled and entangled with each other like a silk weave form (Figure 9b and 9c). After the chemical grafting of PG onto the surface of GO, a significant change was observed. Figure 9d shows morphology of PG-*g*-GO, in which the dark regions are related to the grafted PG onto the GO surface. It is interesting to note that the intensity of the dark color on the basal plane of GO is relatively higher than edges, indicating the higher density of grafted PG on these regions. It can be explained by higher density of hydroxyl functional groups on the basal plane of GO. At higher magnifications (Figure 9e and 9f), arrows marked in the images indicate the thickness increase of GO sheet surface due to the coverage of the PG. Figure 9g shows the morphology of MNP-*i*-PG-*g*-GO hybrid nanostructure. While most of the nanoparticles were immobilized onto the GO, and only few free nanoparticles were observed. It could be noticed that these nanoparticles are homogenously immobilized along with GO layers (Figure 9h). It could be explained that the B-*f*-MNPs are immobilized to the PG-*g*-GO surface via the strong covalent bonding of boroester linkage, rather than being immobilized by simple physical absorption or hydrogen bonding interaction.

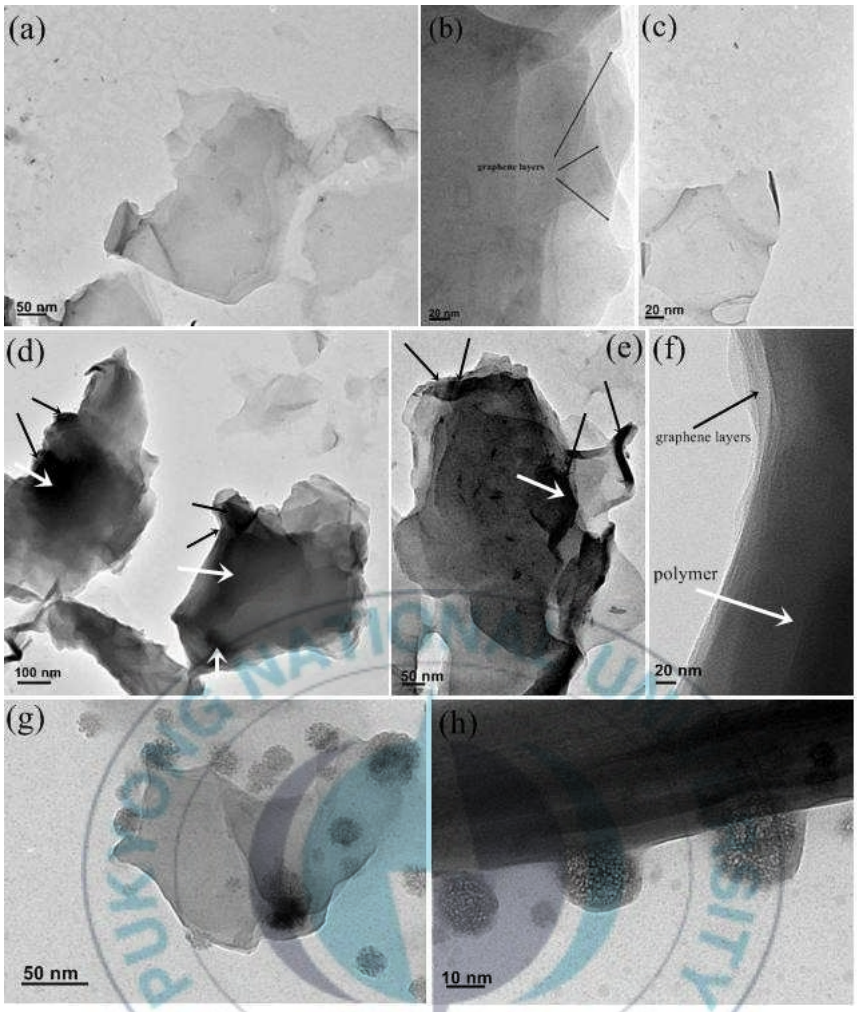

Figure 9. HR-TEM images of (a, b, c) GO, of (d, e, f) PG-*g*-GO and of (g, h) MNPs-*i*-PG-*g*-GO at different magnifications.

2.3.4. Dispersion stability of hybrids in distilled water

To examine the dispersion stability of the hybrid nanostructures, all the samples were dispersed in distilled water at a typical concentration of 0.1mg/mL followed by ultrasonication. The digital photographs provide a vivid observation on the water-dispersible property of the samples as shown in Figure 10. The pristine graphite is not dispersible in water and tends to

form sediments at the bottom of vial or float on top of water due to poor hydrogen-bonding (Figure 10a). On the other hand, GO showed slightly better water-dispersible stability than pristine graphite, indicated by the yellow solution. Unlike pristine graphite, the presence of covalently attached oxygen-containing groups in GO surface such as hydroxyl and carboxyl groups renders it more hydrophilic. However, it is well-known that GO sheets, which have a high specific surface area, tend to form irreversible agglomerates to form graphite via strong π-π stacking and van der Waals interaction, indicating by the presence of solid at the bottom of vial as shown in Figure 10b. In the case of PG-*g*-GO, after the grafting of the PG onto the surface of GO, the dispersibility of the hybrid nanostructure was dramatically increased due to the high hydrophilicity of PG. The homogeneous black color was obvious evidence for the perfect dispersibility in water of the PG-g-GO. The dispersed water solution was stable over 3 months without conspicuous aggregates (Figure 10c). It is also interesting to note that after the immobilization of the B-*f*-MNPs to the PG-*g*-GO, the hybrid nanostructure still remained in well-dispersed state in water as seen in Figure 10d.

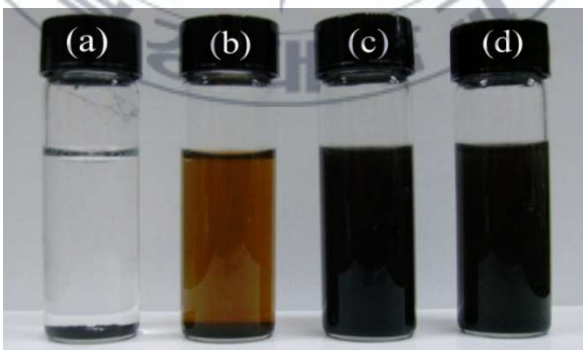

Figure 10. Digital photographs of (a) pristine graphite, (b) GO, (c) PG-g-GO and (d) MNPs-*i*-PG-*g*-GO in distilled water.

Conclusions

In the present study, a facile strategy for the synthesis of water-dispersible graphene based on chemical grafting of PG onto the surface of GO nanosheets is developed. This is the first report on the covalent polymer functionalization of graphene through the facile approach based on in-situ ring-opening polymerization of glycidol. Additionally, the Fe@Au nanoparticles were successfully functionalized using boronic acid through the well-developed Au-S chemistry. Considering a large number of free hydroxyl functional groups appending on the surface of PG-g-GO and B-*f*-MNPs, it is interesting to use prepared PG-g-GO as template for loading magnetic nanoparticles via boroester bonds. The synthesized novel hybrid nanostructures could be stably dispersed in water over three months and emerged as promising materials to meet various requirements for potential applications.

Bibliography

1. C.G. Navarro, M. Burghard and K. Kern, Nano. Lett. 8 (2008) 2045.
2. S. Park, K.S. Lee, G. Bozoklu, W. Cai, S.T. Nguyen and R.S. Ruoff, ACS Nano 3 (2008) 572.
3. J. Wu, W. Pisula, and K. Müllen, Chem. Rev. 107 (2007) 718.
4. C.G. Navarro, R.T. Weitz, A.M. Bittner, M. Scolari, A. Mews, M. Burghard, and K. Kern, Nano. Lett. 7 (2007) 3499.
5. A.A. Balandin, S. Ghosh, W. Bao, I. Calizo, D. Teweldebrhan, F. Miao, and C.N. Lau, Nano. Lett. 8 (2008) 902.
6. J.M. Pereira, P. Vasilopoulos, F.M. Peeters, Nano. Lett. 7 (2007) 946.

7. K.S. Subrahamanyam, S.R.C. Vivekchand, A. Govindaraj, C.N.R. Rao, J. Mater. Chem. 18 (2008) 1517.

8. H. Bai, C. Li, X. Wang and G. Shi, Chem. Commun. 46 (2010) 2376.

9. J.R. Lomeda, C.D. Doyle, D.V. Kosynkin, W. Hwang, J.M. Tour, J. Am. Chem. Soc. 130 (2008) 16201.

10. D. Konatham and A. Striolo, Nano. Lett. 8 (2008) 4630.

11. R. Kou, Y. Shao, D. Wang, M.H. Engelhard, J.H. Kwak, J. Wang, V.V. Viswanathan, C. Wang, Y. Lin, Y. Wang, I.A. Aksay, J. Liu, Electrochem. Commun. 11 (2009) 954.

12. H. Zhang, X. Lv, Y. Li, Y. Wang, and J. Li, ACS Nano 4 (2010) 380.

13. J.D. Fowler, M.J. Allen, V.C. Tung, Y. Yang, R.B. Kaner, and B.H. Weller, ACS Nano 3 (2009) 301.

14. J.T. Robinson, F.K. Perkins, E.S. Snow, Z. Wei, and P.E. Sheehan, Nano. Lett. 8 (2008) 3137.

15. P.K. Ang, W. Chen, A.T.S. Wee, and K.P. Loh, J. Am. Chem. Soc. 130 (2008) 14392.

16. F. Schedin, A.K. Geim, S.V. Morozov, E.W. Hill, P. Blake, M.I. Katsnelson, and K.S. Novoselov, Nat. Mater. 6 (2007) 652.

17. X. Wang, L. Zhi, and K. Müllen, Nano. Lett. 8 (2008) 323.

18. V.Y. Aristov, G. Urbanik, K. Kummber, D.V. Vyalikh, O.V. Molodtsova, A.B. Preobrajenski, A.A. Zakharov, C. Hess, T. Hänke, B. Büchner, I. Vobornik, J. Fujii, G. Panaccione, Y.A. Ossipyan, and M. Knupfer, Nano. Lett. 10 (2010) 992.

19. Z. Liu, Q. Liu, Y. Huang, Y. Ma, S. Yin, X. Zhang, W. Sun, and Y. Chen,

Adv. Mater. 20 (2008) 3924.

20. Q. Liu, Z. Liu, X. Zhang, L. Yang, N. Zhang, G. Pan, S. Yin, Y. Chen, and J. Wei, Adv. Funct. Mater. 19 (2009) 894.

21. C. Di, D. Wei, G. Yu, Y. Liu, Y. Guo, and D. Zhu, Adv. Mater. 20 (2008) 3289.

22. N. Yang, J. Zhai, D. Wang, Y. Chen, and L. Jiang, ACS Nano 4 (2010) 887.

23. J. Yao, X. Shen, B. Wang, H. Liu, G. Wang, Electrochem. Commun. 11 (2009) 1849.

24. G. Wang, X. Shen, J. Yao, J. Park, Carbon 47 (2009) 2049.

25. X. Kang, J. Wang, H. Wu, I.A. Aksay, J. Liu, Y. Lin, Biosen. Bioelectron. 25 (2009) 901.

26. N. Mohanty and V. Berry, Nano. Lett. 8 (2008) 4469.

27. C. Xu and X. Wang, Small 5 (2009) 2212.

28. S. Niyogi, E. Bekyarova, M.E. Itkis, J.L. Mcwilliams, M.A. Hamon, R.C. Haddon, J. Am. Chem. Soc. 128 (2006) 7720.

29. Y. Xu, H. Bai, G. Lu, C. Li, and G. Shi, J. Am. Chem. Soc. 130 (2008) 5856.

30. Q. Yang, X. Pan, F. Huang, and K. Li, J. Phys. Chem. C 114 (2010) 3811.

31. C. Zhu, S. Guo, Y. Fang, and S. Dong, ACS Nano 4 (2010) 2429.

32. H.J. Salavagione, M.A. Gómez, and G. Martínez, Macromolecules 42 (2009) 6331.

33. C. Shan, H. Yang, D. Han, Q. Zhang, A. Ivaska, and L. Niu, Langmuir 25

(2009) 12030.

34. R. Muszynski, B. Seger, and P.V. Kamat, J. Phys. Chem. C 112 (2008) 5263.

35. W. Hong, H. Bai, Y. Xu, Z. Yao, Z. Gu, and G. Shi, J. Phys. Chem. C 114 (2010) 1822.

36. F. Li, H. Yang, C. Shan, Q. Zhang, D. Han, A. Ivaska, and L. Niu, J. Mater. Chem. 19 (2009) 4022.

37. A.H. Lu, E.L. Salabas, and F. Schüth, Angew. Chem. Int. Ed. 46 (2007) 1222.

38. F.F. Fang, H.J. Choi, W.S. Choi, Colloid Polym. Sci. 288 (2010) 359.

39. F.F. Fang, H.J. Choi, and Y. Seo, ACS Appl. Mater. Interf. 2 (2010) 54.

40. S.W. Ko, J.Y. Lim, B.J. Park, M.S. Yang, H.J. Choi, J. Appl. Phys. 105 (2009) 07E703.

41. W. Hummers, R. Offerman, J. Am. Chem. Soc. 80 (1958) 1339.

42. M. Adeli, N. Mirab and F. Zabihi, Nanotechnology 20 (2009) 485603.

43. W.L. Zhou, E.E. Carpenter, J. Lin, A. Kumbhar, J. Sims, and C.J. O'Connor, Eur. Phys. J. D 16 (2001) 289.

44. S.J. Cho, J.C. Idrobo, J. Olamit, K. Liu, N.D. Browning, and S.M. Kauzlarich, Chem. Mater. 17 (2005) 3181.

45. A.L. Korich, K.M. Clarke, D. Wallace, and P.M. Iovine, Macromolecules 42 (2009) 5906.

46. T.A. Pham, S.M. Son, and Y.T. Jeong, Synth. React. Inorg. Met.-Org. Chem. 40 (2010) 216.

47. S. Stankovich, D.A. Dikin, R.D. Piner, K.A. Kohlhaas, A. Kleinhamma, Y. Jia, Y. Wu, S.T. Nguyen, R.S. Ruoff, Carbon 45 (2007) 1558.

48. C. Siegers, M. Bielsalski and R. Haag, Chem. Eur. J. 10 (2004) 2831.

49. M. Fang, K. Wang, H. Lu, Y. Yang and S. Nutt, J. Mater. Chem. 19 (2009) 7098.

CHAPTER 3

Facile covalent immobilization of cadmium sulfide quantum dots on graphene oxide nanosheets: Preparation, characterization, and optical properties*

A facile approach for the preparation of novel hybrid material containing graphene and an inorganic semiconducting material, cadmium sulfide quantum dots (CdS QDs) is demonstrated for the first time. First, amino-functionalized CdS QDs were prepared by modifications of the kinetic trapping method. Then, pristine graphite was oxidized and exfoliated to obtain graphene oxide nanosheets (GONS), which further were acylated with thionyl chloride to introduce acyl chloride groups on their surface. Subsequently, the immobilization of CdS QDs on GONS surface was obtained through an amidation reaction between amino groups located on CdS QDs surface and acyl chloride groups bound to GONS surface. Fourier transform infrared spectroscopy (FT-IR), ^{1}H nuclear magnetic resonance (^{1}H-NMR), X-ray diffraction (XRD), X-ray photoelectron spectroscopy (XPS), energy dispersive X-ray (EDX) spectroscopy were employed to investigate the changes in surface functionalities, while high resolution transmission electron microscopy (HR-TEM) and field emission scanning electronic microscopy (FE-SEM) were used to study the morphologies and distribution of CdS QDs onto GONS surface. Thermogravimetric analysis (TGA) was employed to characterize the weight loss of the samples on heating. Photoluminescence (PL) measurements were used to study optical properties of prepared CdS QDs and CdS-graphene hybrid material.

---

*This work was published in **Nanotechnology, 2010, 21, 465603.**

3.1. Introduction

The recent increase of interest in carbon-based hybrid materials and the continuous progress of nanotechnology in materials science have opened new ways for the development arrays of novel functional materials. Among them, Graphene, a flat monolayer of hexagonally arrayed sp^2-bonbed carbon atoms tightly packed into a two-dimensional (2D) honeycomb lattice, has been emerging as a fascinating material for a wide variety of potential applications in large scale transistor fabrication [1], position sensitive IR detector [2], photovoltaic [3, 4], chemical sensor [5], catalyst support [6], Li ion batteries [7] because of its remarkable thermal, chemical, physical and electrical properties [8-12] since its discovery in 2004. While these proposed protocols have triggered burgeoning interest, the realization of these potential applications are limited due to the difficulties in isolation and fabrication which still poses practical challenges that must be addressed. Recently, researchers have circumvented these obstacles by using solution based processing technique [9, 10]. In this regard, the chemical transformation of pristine graphite to graphite oxide (GO), which can be easily exfoliated in solution to yield stable dispersions consisting monolayer, bilayer or few layer sheets of graphene oxide nanosheets (GONS) is the most effective procedure. Additionally, the presence of covalently attached oxygen-containing groups such as hydroxyl; epoxy groups on the basal plane and carboxyl groups at the edge of GONS surface provides a handle for further surface chemical functionalizations via well-developed carbon surface chemistry. Therefore, these stable flexible GONS are often used as the starting material for preparation of graphene-based hybrid materials.

Recently, the combination of carbon family materials with quantum dots (QDs) is expected to improve the prospects for using hybrid materials

in optoelectronic applications. With this in mind, several strategies have been developed for functionalizing the carbon family material with QDs to obtain new optoelectronic materials [11-13]. As a novel carbon nanomaterial, graphene is highly expected as a potential nanoscale building block for developing such hybrid materials because it possesses large interfacial surface area as well as the superior electrical conductivity far much better than its analogous counterpart, carbon nanotubes (CNTs) [14]. Additionally, its inexpensive sources (graphite) and the two-dimensional nanostructure have led to the rise of scientific investigations among researchers in employing them as a cheap substitute for CNTs to capture and transport electrons from excited QDs for generating novel optoelectronic materials. Hence, it is believed that hybrids containing graphene and QDs would have better performances in optoelectronic applications in comparison with CNTs-QDs hybrid materials. However, up to now, although a number studies have been reported for the fabrication of CNTs-based materials with QDs [15-20], only a few studies have been concerned with the synthesis of hybrid materials containing graphene and QDs [21-25].

Among the most investigated inorganic semiconductor nanoparticles, CdS QDs have attracted tremendous attention for many potential applications due to their outstanding properties, including discrete energy bands and narrow emission profiles [22, 23]. However, up to date, reports on the immobilization of CdS QDs on graphene surface are relatively rare. For example, Cao *et al* [24] have synthesized graphene-CdS nanocomposites by a one-step method in dimethyl sulfoxide (DMSO). According to their results, the graphene–CdS hybrids exhibited good optoelectronic properties and the stable single layer property of graphene to guarantee the final graphene-CdS product in a single-layer form. Feng *et al*

[25] have reported on the preparation of graphene nanosheets decorated with tiny CdS QDs by a facile approach via π-π stacking interaction using benzyl mercaptan as the interlinker. Their approach displayed excellent nonlinear optical properties. More recently, Chang *et al* [26] synthesized hybrid containing graphene and CdS QDs by *in situ* growth of CdS QDs on noncovalently functionalized graphene. Their hybrids showed enhanced photocurrent generation capability and incident photon-to-electron conversion efficiency at visible light. Although these approaches exhibited some achievements in the field of novel optoelectronic materials, there is still one drawback that must be overcome to meet requirements for practical applications. The drawback is that CdS QDs may easily leach out from graphene during application due to weak interactions between GONS and CdS QDs in synthesized hybrids by above mentioned methods are poor interactions, such as electrostatic interaction, π-π stacking interaction. Hence, a new approach is essential to develop a convenient and applicable synthesis for preparation novel hybrid materials in which CdS QDs were immobilized on graphene surface by strong interaction for potential optoelectronic applications.

On the basis of these observations, herein, we have developed a simple approach for fabrication of a novel hybrid material containing CdS QDs and graphene through an amidation reaction for the first time. To the best of our knowledge, the covalent immobilization of CdS QDs onto the surface of GONS by amidation reaction to yield novel optoelectronic materials has not been reported yet. In our approach, pristine graphite was oxidized by the modified Hummer's method [27] and then exfoliated to generate GONS by ultrasonication, which was further acylated with thionyl chloride to give acyl chloride-bound GONS. The amino-functionalized CdS

QDs were synthesized using 4-aminothiophenol by modifications of the kinetic trapping method of Herron *et al* [28]. Subsequently, the covalent immobilization of CdS QDs to GONS was carried out by covalent bonding through the simple amidation reaction.

3.2. Experimental section

3.2.1. Materials

Graphite powder from Sigma-Aldrich was used to prepare GO. Cadmium acetate dihydrate, 4-aminothiophenol (4-ATP), sodium sulfide and other chemicals were purchased from Sigma-Aldrich and used as received. Tetrahydrofuran (Junsei, Japan) and thionyl chloride (Duksan Pure Chemical, South Korea) were distilled prior to use. All other solvents were purchased from Sigma-Aldrich and used as received unless otherwise stated.

3.2.2. Synthesis of 4-aminothiophenol-functionalized CdS QDs (4-ATP-*f*-CdSQDs)

Sodium sulfide (1.68 g) and 4-aminothiophenol (2.46g) was dissolved in 1:1:2 (v/v) acetonitrile/methanol/water solvents mixture (80 mL). Then, the solution was added to a rapidly stirring solution of cadmium acetate dihydrate (2.52 g) in the same solvent under nitrogen atmosphere. The solution turns yellow, indicating the formation of CdS nanoparticles. After vigorous stirring for 12h at room temperature, the solvent was removed by distillation under decreased pressure. The solid was separated by centrifugation and subsequently washed repeatedly using water, acetone, and diethyl ether. The product was dried in vacuum oven for 24 h to obtain the pure product as a yellow solid.

3.2.3. Synthesis of GONS

In a typical synthetic process, natural graphite powder (2.0g) was added to cooled (0°C) H_2SO_4 (350 mL). Then, $KMnO_4$ (20 g) and $NaNO_3$ (3 g) were added gradually while stirring. The mixture was then transferred to a 30°C water bath and stirred for 20 min. De-ionized water (250 mL) was slowly added and the temperature was increased to 98°C. The mixture was maintained at that temperature for 30 min. The reaction was terminated by adding de-ionized water (500 mL) followed by adding H_2O_2 solution (40 mL, 30%). The color of the mixture changed to brilliant yellow, indicating the oxidation of pristine graphite to GO. Then, the mixture was filtered and washed with diluted HCl to remove metal ions. Finally, the product was washed repeatedly with distilled water until the pH was 7. The sample of GO was obtained after drying. To prepare GONS, the as-obtained GO was re-dispersed in distilled water to create a yellow-brown dispersion, and the exfoliation of GO to generate GONS was achieved by ultrasonication for 30 min. The resultant aqueous dispersion of brown GONS was stable.

3.2.4. Synthesis of acyl chloride-functionalized GONS (GONS-COCl)

GONS (300 mg) was stirred with an excess amount of thionyl chloride (50 mL) under nitrogen atmosphere for 24h at 80°C. The GONS-COCl were vacuum filtered using PTFE membrane and completely rinsed with distilled tetrahydrofuran (THF) to prevent hydrolysis of the –COCl functional groups. Subsequently, the GONS-COCl was stored under nitrogen to prevent any hydrolysis and was used immediately for further reactions.

3.2.5. Preparation of CdS-immobilized GONS (CdS-*i*-GONS)

For the covalent immobilization of CdS QDs on GONS surface, the GONS-COCl (100 mg) was first suspended in distilled THF (30 mL). Then, the 4-ATP-*f*-CdSQDs (5 mg) was added to the solution while stirring under nitrogen atmosphere at room temperature. The reactive –COCl groups of the GONS-COCl react the $–NH_2$ groups of the 4-ATP-*f*-CdSQDs and are linked via an amide bond. After continuous stirring for 24h, the product was separated using PTFE filter membrane system, washed with distilled water and diethyl ether. Then, the product was dried in the vacuum oven at 40^oC overnight to obtain CdS-*i*-GONS powder.

3.2.6. Characterization techniques

^1H nuclear magnetic resonance (^1H-NMR) spectrum was recorded using a JEOL JNM ECP 400 spectrophotometer. HR-TEM images were recorded using Joel JEM 2010 instrument (Japan) with an accelerating voltage of 200KV to observe the nanoscale structures, by placing a drop of the samples dispersed in ethanol on copper grids and drying. The morphology and elemental analysis of the hybrids were carried out by using FE-SEM images equipped with an EDX spectrometer (Hitachi JEOL-JSM-6700F system, Japan). The changes in the surface chemical bondings were recorded by FT-IR (Perkin-Elmer Spectroscopy GX, USA), in the frequency range of 500-4000cm^{-1}. Surface composition was investigated using X-ray photoelectron spectroscopy (Thermo VG Multilab 2000) in ultra high vacuum with Al *Kα*. The crystallographic states of the samples were determined by a Philips X'pert-MPD system diffractometer (Netherland) with Cu *Kα* radiation. Thermal studies of the materials were carried out on a Perkin-Elmer (USA) Pyris 1 analyzer. The samples were scanned within the temperature range from 50 to 700^oC at heating rate of 10^oC min^{-1} under

continuous nitrogen flow. PL spectra were recorded on F-4500 spectrofluorometer (Hitachi, Japan).

3.3 Results and discussion

3.3.1. Characterization of the 4-ATP-*f*-CdSQDs

The synthetic route of the 4-ATP-*f*-CdSQDs is shown in Scheme 1. The surface functionalization, bonding nature, and morphologies of 4-ATP-*f*-CdSQDs were characterized using various techniques. Figure 1(a) shows ^{1}H-NMR spectrum (DMSO, 400MHz) of 4-ATP-*f*-CdSQDs, which clearly indicates the binding of 4-ATP to the surface of CdS QDs. On the other hand, figure 1(b) shows the IR spectrum of 4-ATP-*f*-CdSQDs. As can be seen from figure 1(b), the peaks at 3336 cm^{-1} and 3210 cm^{-1} could be assigned to the N-H stretching band, while strong peak at 1622 cm^{-1} could be related to N-H bending band of the primary amine groups on the surface of CdS QDs. The peaks at 1489 and 1177 cm^{-1} are assigned to stretching vibration of the aromatic (C=C) and C-N bonding of 4-ATP located on CdS QDs surface, respectively.

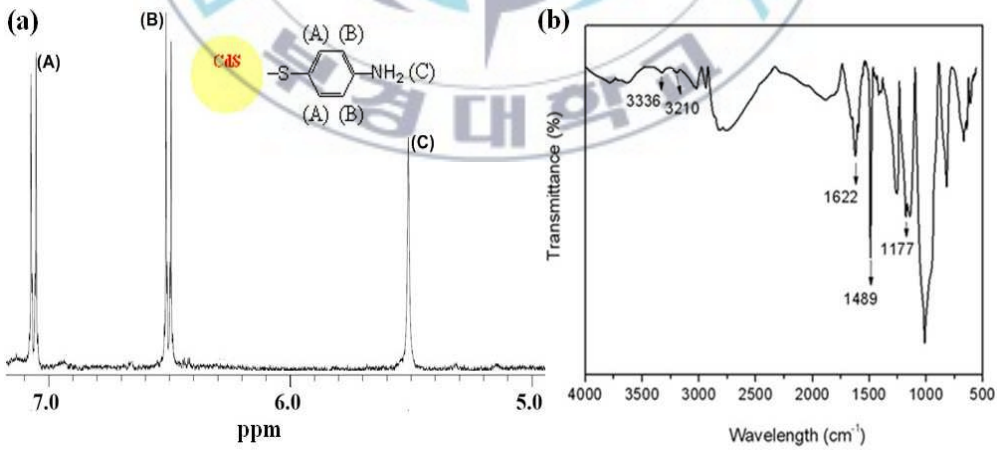

Figure 1. (a) ^{1}H-NMR spectrum (DMSO) and (b) FT-IR spectrum of 4-ATP-*f*-CdSQDs.

In order to better understand the chemical composition of synthesized 4-ATP-*f*-CdSQDs, EDX spectrum of the sample was recorded as shown in figure 2. The spectrum clearly details the presence of cadmium composition along with sulfur and nitrogen. These results clearly indicate that 4-ATP was bound to the surface of CdS QDs after the surface modification process. On the other hand, the morphologies of 4-ATP-*f*-CdSQDs were studied by FE-SEM and HR-TEM images as shown in figure 3. The particle size of CdS QDs is about 16-20 nm. It was interesting to note that CdS QDs tend to aggregate into clusters, which could be due to the binding of 4-ATP to the CdS QDs surface.

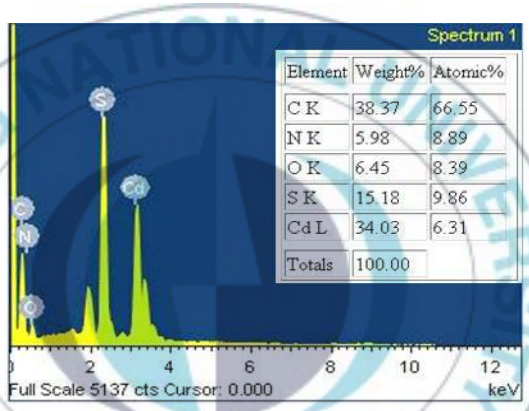

Figure 2. (a) EDX spectrum of 4-ATP-*f*-CdSQDs.

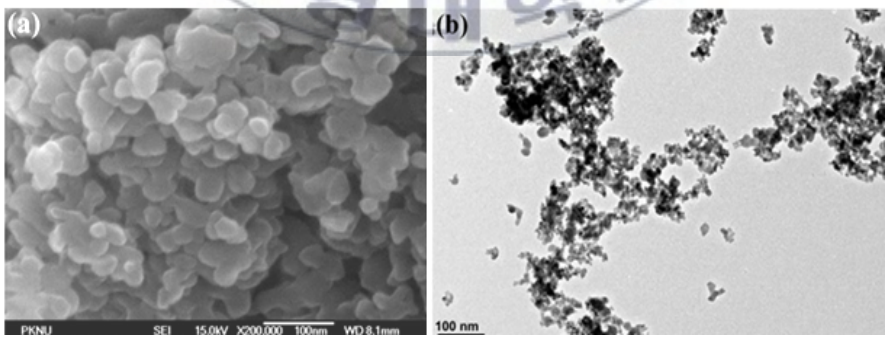

Figure 3. (a) FE-SEM image and (b) HR-TEM image of 4-ATP-*f*-CdSQDs.

3.3.2. The immobilization of 4-ATP-*f*-CdSQDs on the GONS surface (CdS-*i*-GONS)

The procedure for covalent immobilization of CdS QDs onto the GONS surface is illustrated in Scheme 2. The three-step process includes: (1) the GONS was prepared by oxidizing graphite followed by exfoliation in ultrasonication bath, (2) the prepared GONS was converted to the GONS-COCl by suspending the GONS in solution of thionyl chloride at 80^{o}C, (3) the immobilization of CdS QDs onto the GONS surface was carried out via an amidation reaction between amino group of 4-ATP-*f*-CdSQDs and acyl chloride groups of GONS-COCl.

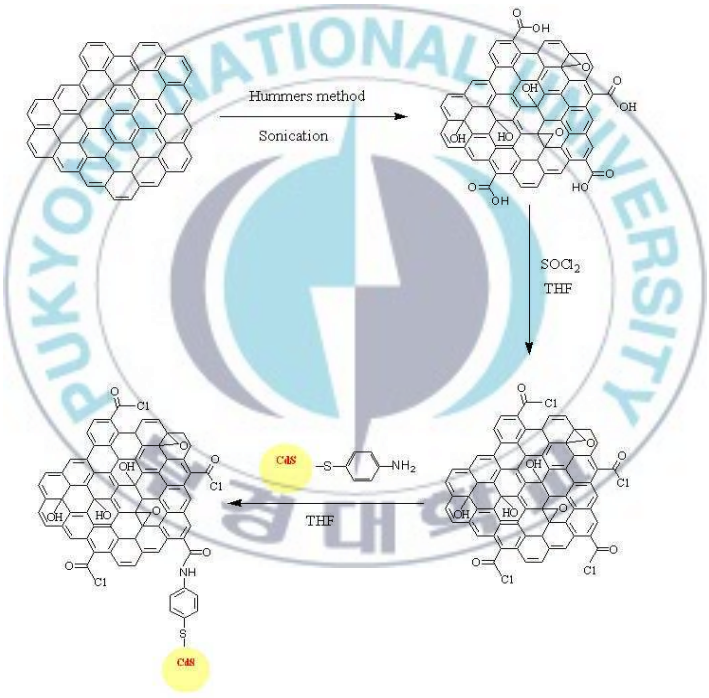

Scheme 2. Schematic illustration on the preparation of hybrid material by the covalent immobilization of CdS QDs onto the surface of GONS.

Figure 4 shows FT-IR spectra of the pristine graphite, GO and CdS-*i*-GONS hybrid, which obtained at different processing step. In the spectrum of pristine graphite (figure 4(a)), the peaks at 3021 and 1548 cm^{-1} are assigned

to C-H stretching and C=C stretching vibration of aromatic ring, respectively. The FT-IR spectrum of GO differs from that of pristine graphite as shown in figure 4(b). The oxygen-containing functional groups of GO were revealed via the peaks at 1240, 1365, and 1729 cm^{-1}, which correspond to C-O-C stretching vibrations, C-OH bending and C=O stretching of carboxylic acid, respectively. Furthermore, the broad band at 3369 cm^{-1} could be assigned to stretching of the –OH groups on the GO surface, while the peak at 1569 cm^{-1} relates to C=C stretching of aromatic ring. For the spectrum of CdS-*i*-GONS (figure 4(c)), it is interesting to note that the peaks at 1729 and 1365 cm^{-1} almost disappears. The new peaks emerge at 1622 and 3437 cm^{-1} are assigned to the C=O characteristic stretching and N-H stretching of the amide groups on the GONS surface, respectively. Whereas the feature peaks of graphitic structure of the CdS-*i*-GONS still appear at1489 and 3022 cm^{-1}. These results clearly indicate that the 4-ATP-*f*-CdSQDs were covalently immobilized on GONS surface through the amidation reaction.

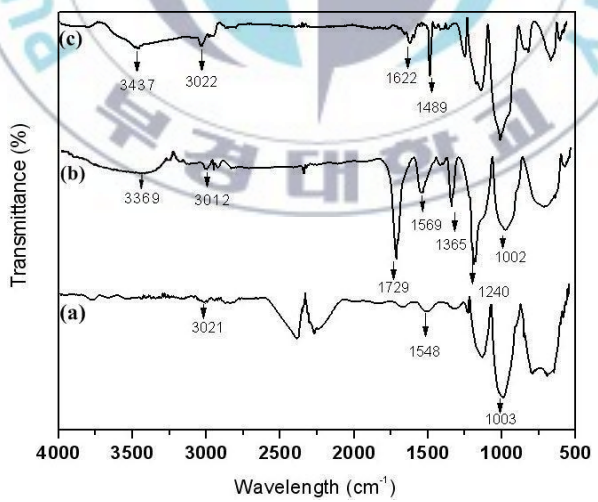

Figure 4. FT-IR spectra of (a) pristine graphite, (b) GO, and (c) CdS-*i*-GONS.

XRD is an effective method to investigate the interlayer changes and the crystalline properties of synthesized material. Figure 5 shows the XRD patterns of pristine graphite, GO, CdS-*i*-GONS, and 4-ATP-*f*-CdSQDs. The strong peak in the XRD pattern of pristine graphite appears at $2\theta = 26.6^{o}$, corresponding to the interlayer spacing of 0.25 nm (figure 5(a)). The GO pattern shows a characteristic peak at $2\theta = 11.8^{o}$, corresponding to interlayer spacing of 0.44 nm, indicating the presence of oxygen-containing functional groups, which formed during oxidation (figure 5(b)). The groups cause the GO sheets to stack more loosely, and the interlayer spacing increases from 0.25 nm to 0.44 nm [29]. After the binding of CdS QDs to GONS surface, significant changes were observed in XRD pattern of the sample (figure 5(c)). It is well-known that the attached nanoparticles may prevent the restacking of carbon sheets, and therefore the characteristic diffraction peaks of the layered structure disappear. However, in this case, the feature diffraction peak of GO that appears at 11.8^{o} was still observed in CdS-*i*-GONS. The XRD pattern of CdS-*i*-GONS only shows the relative decrease in the intensity of the diffraction peak at $2\theta = 11.8^{o}$ in comparison with that of the GO in the same test conditions, indicating the incomplete exfoliation of GO to generate GONS through ultrasonication within a short period. All the other diffraction peaks appear at $2\theta = 23$, 42.8 and 51.6^{o} can be unambiguously indexed to the (111) plane, (220) plane and (311) plane of the cubic CdS, respectively, which are in good agreement with the standard values in the standard card of CdS (JCPDS 10-0454). Furthermore, XRD pattern of 4-ATP-*f*-CdSQDs was obtained as shown in figure 5(d). It can be clearly seen that diffraction peaks of CdS plane appear with a weak intensity, which could be due to the binding of 4-ATP to CdS QDs surface after the modification process. The results clearly confirm that CdS QDs were

successfully immobilized on the GONS surface.

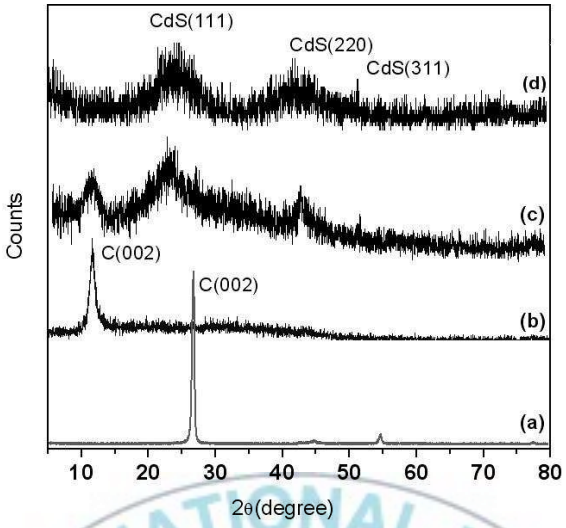

Figure 5. XRD patterns of (a) pristine graphite, (b) GO, (c) CdS-*i*-GONS, and (d) 4-ATP-*f*-CdSQDs.

In order to better understand the chemical composition of the prepared hybrid, EDX spectra of GO and CdS-*i*-GONS hybrid samples were recorded as shown in figure 6. In comparison with that of GO sample, EDX spectrum of CdS-*i*-GONS shows the presence of cadmium, sulfur, and nitrogen elements. These characterizations proved the successful immobilization of CdS QDs onto the surface of GONS.

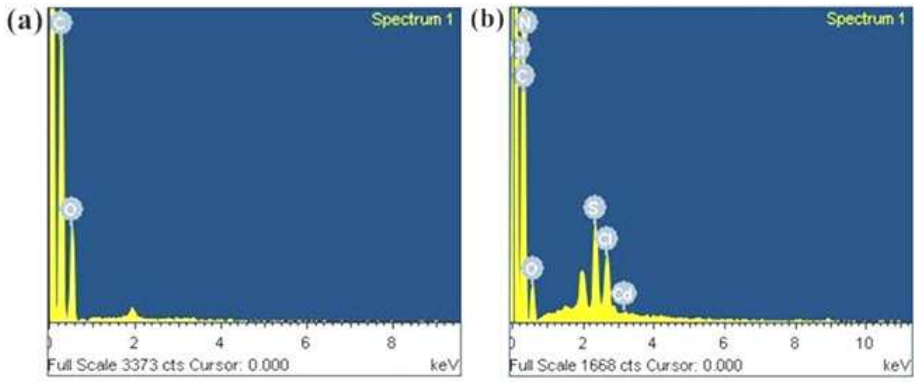

Figure 6. EDX spectra of (a) GO and (b) CdS-*i*-GONS.

XPS is one of the surface analytical techniques, which can provide useful information on the nature of the functional groups and also on the chemical composition of the surfaces. In order to identify the surface elements, a full XPS spectrum in the binding energy (BE) range 0-700 eV of the CdS-*i*-GO sample was recorded and shown in figure 7(a). The existence of carbon (C 1s), sulfur (S 2p), cadmium (Cd 3d), oxygen (O 1s), nitrogen (N 1s) in the sample can be clearly seen. To obtain clear information about the functional groups that correspond to carbon atoms, the C 1s peak of the sample was shown in detail (figure 7(d)). The C 1s spectrum of the sample could be deconvoluted into three peaks. The main peak of C 1s located at 285.03 eV is attributed to the sp^2 carbon of C=C bonding in the graphitic structure, whereas the other two peaks at 286.85 eV and 288.73 eV are assigned to carbon atoms in amide (N-C=O) and carboxyl (O=C-OH) functional groups, respectively. Moreover, the O 1s spectrum shows several peaks which correspond to different oxygen-containing functional groups on the sample surface (figure 7(e)). The peaks are assigned to amide group (O=C-N) at 531.27 eV, hydroxyl group (C-OH) at 532.39 eV, ester group (O-C=O) at 533.42 and 534.92 eV, [30]. These results are consistent with

the FT-IR, XRD and EDX analysis as mentioned above, which further confirm the binding of 4-ATP-*f*-CdSQDs to the surface of GONS.

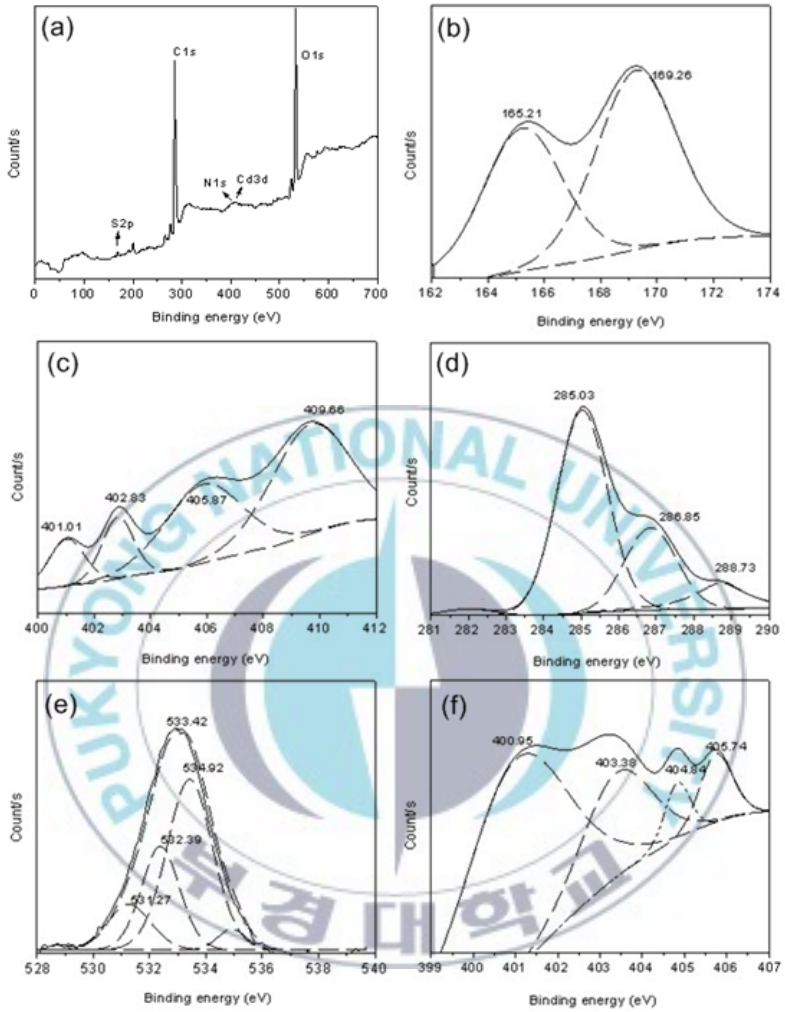

Figure 7. XPS spectra of CdS-*i*-GONS: (a) Full XPS spectrum of a typical sample, (b) S2p, (c) Cd3d, (d) C1s, (e) O1s, (f) N1s spectral regions in detail.

3.3.3. Morphologies of hybrid material

The morphologies of pristine graphite and GO were investigated by FE-SEM techniques as shown in figure 8. The images were recorded directly using the prepared powdered samples. It can be noticed that pristine graphite has a laminated structure in which a large amount of sheets are stack together (figure 8(a)). In comparison with GO, because of oxidation, the GO sheets break into pieces smaller than pristine graphite, which was clearly observed in the images (figure 8(b)).

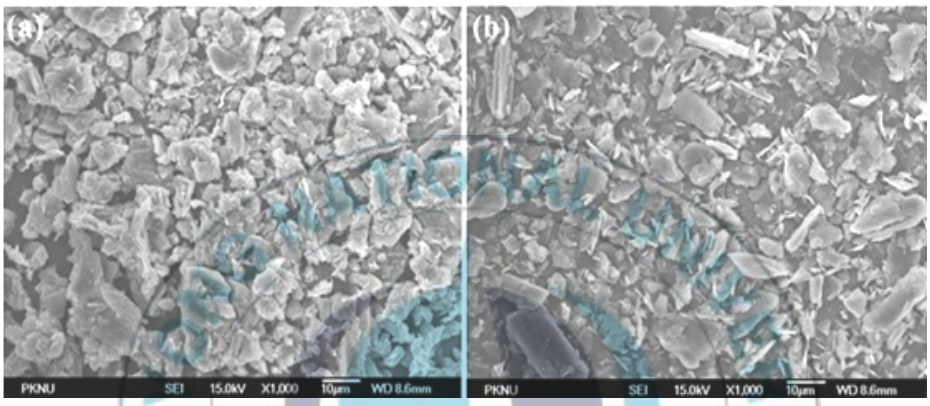

Figure 8. FE-SEM images of (a) pristine graphite, and (b) GO.

In order to further investigate the morphology of the prepared materials, HR-TEM images were recorded. The morphologies of the prepared GONS samples dispersed in ethanol were obtained as shown in figure 9(a-c). The presence of a mixture of graphene layers was observed (marked by arrows). Most of the layers are bilayer and few layer graphene are present. They are typically curved, like wrinkled morphology due to the presence of functional groups and extremely small thickness of the GONS. The images of the edges of a typical graphene flakes showing graphene layers which were transparent and entangles with each. The inset image shows the measured selected area electron diffraction pattern (SAED),

which is typical for few-layered GONS. The direct evidence for the immobilization of CdS QDs onto the GONS surface was given by HR-TEM images in figure 9(d-f). Most of the CdS QDs were well immobilized onto the GONS surface, only few free CdS QDs were observed in figure 9(e) (marked in red circle). It could be explained that CdS QDs were immobilized onto GONS surface via strong bonding of amide linkages.

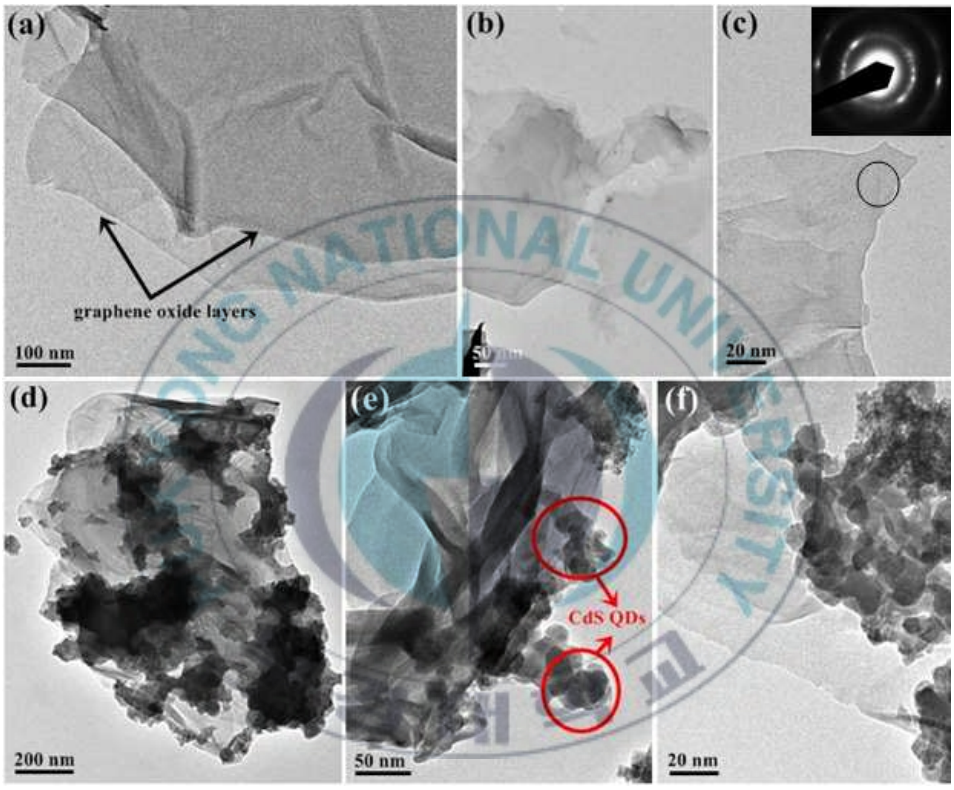

Figure 9. HR-TEM images of (a-c) GONS, and (d-f) CdS-*i*-GONS at different magnifications. Inset image in (c) represents the corresponding SAED pattern of the circled area.

3.3.4. Thermal stability of hybrid material

In order to study the thermal behavior and stability of graphene-based hybrid material after chemical modification, TGA of the samples were

conducted as shown in figure 10. It was observed that pristine graphite was more stable and no dramatic mass loss was detected when it was heated up to 700^{o}C. Pristine graphite shows only a little mass loss which is about 2% of its total weight below 700^{o}C, which could be due to moisture present in the pristine graphite. On the other hand, GO is thermally unstable and starts to lose mass upon heating even below 100^{o}C due to the removal of physically adsorbed water. The major mass loss of GO occurs at 180^{o}C and loses to 98% of its total mass, which could be attributed to the pyrolysis of the labile oxygen-containing functional groups, yielding CO, CO_2 and steam [31]. Comparing with GO, the thermal stability of the CdS-*i*-GONS hybrid is higher than that of GO. TGA traces of the CdS-*i*-GONS shows a gradual mass loss, which is about 40% of its total mass in the entire temperature range. This suggests that CdS QDs was well immobilized to the GONS surface, which leads to improve the thermal stability in the hybrid material.

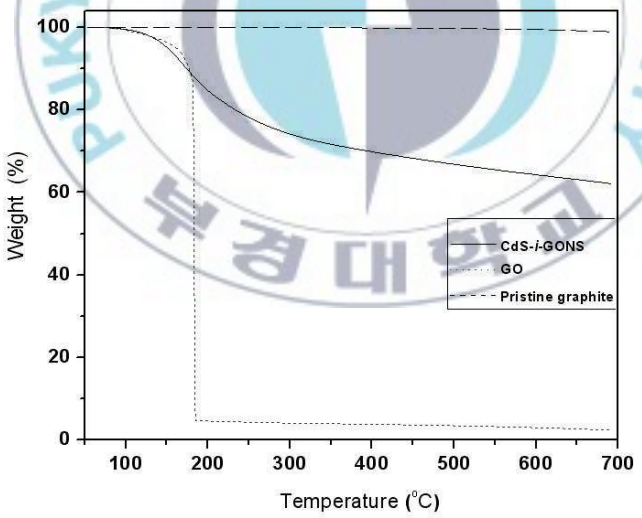

Figure 10. TGA curves of pristine graphite (dash line), GO (dot line), and CdS-*i*-GO (solid line).

3.3.5. Optical properties of hybrid material

The optical properties of 4-ATP-*f*-CdSQDs and CdS-*i*-GO hybrid were studied by PL spectroscopy as shown in figure 11. It is interesting to note that the characteristic emission of both samples shows two emission bands when excited at 254 nm. The first peak of CdS QDs appears in the region of 405 nm, which is close to the band edge emission, whereas the second peak is around 540 nm. It is also worth to note that the first peak is sharp and exhibits a blue shift in energy with decreasing QDs size, the second peak is a broad emission and does not show any systematic dependence on the QDs size, which have been reported by several previous studies [32-35]. The inset image provides a vivid observation on the color change of the prepared 4-ATP-*f*-CdSQDs illuminated under an ultraviolet (UV) lamp. On the other hand, after the attachment of CdS QDs to GONS surface, a significant change was observed in the PL spectrum of CdS-*i*-GONS. The relative decrease in the intensity of emission bands indicates efficient electron transfer from QDs to graphene. These results demonstrate the new class of graphene-based semiconductor hybrid material developed by our approach could provide new opportunities for researchers in designing novel hybrid material for optoelectronic applications.

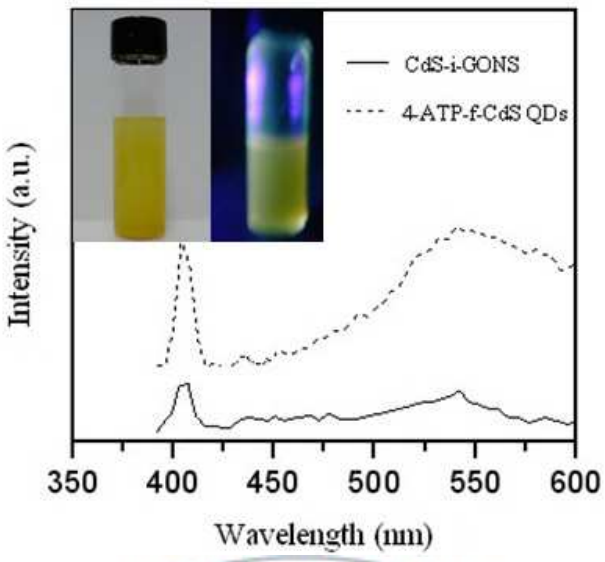

Figure 11. (a) PL spectra of 4-ATP-*f*-CdSQDs (dash line) and CdS-*i*-GO in DMSO at room temperature (λ_{ex}= 254nm) (solid line). The inset image shows the color of prepared 4-ATP-*f*-CdSQDs in DMSO under room light (left) and UV lamp (right).

Conclusion

In the present study, the optoelectronic hybrid material of CdS QDs and GONS was successfully prepared through a simple amidation reaction for the first time. The main advantage of this approach is that CdS QDs are strongly bonded to the surface of GONS by covalent bonding, which guarantees the efficient optoelectronic properties of CdS-*i*-GONS hybrid and opens new pathways for the development of optoelectronic hybrid materials containing graphene and QDs. Considering the optical importance of CdS QDs as well as the unique properties and inexpensive source of graphene, in future, these materials are expected to provide a cost-effective platform for many optoelectronic applications such as solar energy conversion, photonic devices, sensor or catalysts

Bibliography

1. D. Joung, A. Chunder, L. Zhai and S.I. Khondaker, Nanotechnology 21 (2010) 163109.
2. S. Ghosh, B.K. Sarker, A. Chunder, L. Zhai, and S.I. Khondaker, Appl. Phys. Lett. 96 (2010) 163109.
3. Q. Liu, Z. Liu, X. Zhang, N. Zhang, L. Yang, S. Yin, and Y. Chen, Appl. Phys. Lett. 92 (2008) 223303.
4. J. Wu, H.A. Becerril, Z. Bao, Z. Liu, Y. Chen, and P. Peumans, Appl. Phys. Lett. 92 (2008) 263302.
5. J.D. Fowler, M.J. Allen, V.C. Tung, Y. Yang, R.B. Kaner, and B.H. Weller, ACS Nano 3 (2009) 301.
6. R. Kou, Y. Shao, D. Wang, M.H. Engelhard, J.H. Kwak, J. Wang, V.V. Viswanathan, C. Wang, Y. Lin, Y. Wang, I.A. Aksay, J. Liu, Electrochem. Commun. 11 (2009) 954.
7. G. Wang, X. Shen, J. Yao, J. Park, Carbon 47 (2009) 2049.
8. S. Park, K.S. Lee, G. Bozoklu, W. Cai, S.T. Nguyen, and R.S. Ruoff, ACS Nano 2 (2008) 572.
9. J. Wu, W. Pisula, and K. Müllen, Chem. Rev. 107 (2007) 718.
10. C.G. Navarro, M. Burghard, and K. Kern, Nano Lett. 8 (2008) 2045.
11. A.A. Balandin, S. Ghosh, W. Bao, I. Calizo, D. Teweldebrhan, F. Miao, C.N. Lau, Nano Lett. 8 (2008) 902.
12. C.G. Navarro, R.T. Weitz, A.M. Bittner, M. Scolari, A. Mews, M. Burghard, and K. Kern, Nano Lett. 7 (2007) 3499.

13. S. Niyogi, E. Bekyarova, M.E. Itkis, J.L. McWilliams, M.A. Hamon and R.C. Haddon, J. Am. Chem. Soc. 128 (2006) 7720.

14. J. Shen, Y. Hu, C. Li, C. Qin, and M. Ye, Small 5 (2009) 82.

15. J. M. Haremza, M. A. Hahn, and T. D. Krauss, Nano Lett. 2 (2001) 1253.

16. S. Ravindran, S. Chaudhary, B. Colburn, M. Ozkan, C.S. Ozkan, Nano Lett. 3 (2003) 447.

17. M. Grzelczak, M. A. Correa-Duarte, V. Salgueiriño-Maceira, M. Giersig, R. Diaz and L. M. Liz-Marzán, Adv. Mater. 18 (2006) 415.

18. S. Stankovich, D. A. Dikin, H. B. Dommett Geoffrey, K. M. Kohlhaas, E. J. Zimney, E. A. Stach, R. D. Piner, S. T. Nguyen, and R. S. Ruoff, Nature 442 (2006) 282.

19. M. J. Biercuk, S. G. Mason, J. M. Chow, and C. M. Marcus, Nano Lett. 5 (2005) 1267.

20. N. Zhang, J. Sun, D. Jiang, T. Feng, Q. Li Carbon 47 (2009) 1214.

21. X. Lim, Y. Zhu, F. C. Cheong, N. M. Hanafiah, S. Valiyaveettil, ACS Nano 2 (2008) 1389.

22. H. Dong, W. Gao, F. Yan, H. Ji, and H. Ju, Anal. Chem. 82 (2010) 5511.

23. Y. Wang, J. Lu, L. Tang, H. Chang, and J. Li, Anal. Chem. 81 (2009) 9710.

24. Y.T. Kim, J.H. Han, B.H. Hong, and Y.U. Kwon, Adv. Mater. 22 (2010) 515.

25. X. Geng, L. Niu, Z. Xing, R. Song, G. Liu, M. Sun, G. Cheng, H. Zhong, Z. Liu, Z. Zhang, L. Sun, H. Xu, and L. Liu, Adv. Mater. 22 (2010) 638.

26. N. Jia, Q. Lian, Z. Tian, X. Duan, M. Yin, L. Jing, S. Chen, H. Shen, and M. Gao, Nanotechnology 21 (2010) 045606.

27. B. Pan, D. Cui, R. He, F. Gao, Y. Zhang, *Chem. Phys. Lett.* 417 **(**2006) 419.

28. L. Stobinski, J. Perzy, P. Tomasik, H. M. Lin, *J. Alloys Comd.* 445 (2008) 137.

29. Y. T. Kim, J. H. Han, B. H. Hong, and Y. U. Kwon, Adv. Mater. 22 (2010) 515.

30. W. X. Zhao, Z. P. Bai, A. L. Ren, B. Guo, C. Wu, Appl. Surf. Sci. 256 (2010) 3493.

31. J. Nayak, S. N. Sahu, J. Kasuya, S. Nozaki, Appl. Surf. Sci. 254 (2008)7215.

32. A. Cao, Z. Liu, S. Chu, M. Wu, Z. Ye, Z. Cai, Y. Chang, S. Wang, Q. Gong, and Y. Liu, Adv. Mater. 22 (2010) 203.

33. M. Feng, R. Sun, H. Zhan, and Y. Chen, Nanotechnology 21 **(**2010) 075601.

34. H. Chang, X. Lv, H. Zhang, J. Li, Electrochem. Commun. 12 (2010) 483.

35. W. Hummers, R. Offerman, J. Am. Chem. Soc. 80 (1958) 1339.

36. N. Herron, Y. Wang, and H. Eckert, J. Am. Chem. Soc. 112 (1990) 1322.

37. M. Fang, K. Wang, H. Lu, Y. Yang, S. Nutt, J. Mater. Chem. 19 (2009) 7098.

38. P. G. Rouxhet, A. M. Misselyn-Bauduin, F. Ahimou, M. J. Genet, Y. Adriaensen, T. Desille, P. Bodson, and C. Deroanne Surf. Interface Anal. 40 (2008)718.

39. S. Stankovich, D. A. Dikin, R. D. Piner, K. A. A. Kohlhass Kleinhammes, Y. Jia, Y. Wu, Carbon 45 (2007) 1558.

40. P. Nandakumar and Vijayan , *J. Appl. Phys*. 91 (200) 1509.

41. P. Thangadurai, S. Balaji, P. T. Manoharan, Nanotechnology 19 **(**2008) 435708

42. F. Wang, G. Xu, Z. Zhang, and X. Xin, Eur. J. Inorg. Chem. 1 (2006) 109.

43. P.K. Khanna, N. Singh, *J. Lumines.* 127 (2007) 474.

CHAPTER 4

A simple approach for immobilization of gold nanoparticles on graphene oxide sheets by covalent bonding*

In this chapter, amino – functionalized gold nanoparticles with a diameter of around 5 nm were immobilized onto the surface of graphene oxide sheets (GOS) by covalent bonding through a simple amidation reaction. Pristine graphite was firstly oxidized and exfoliated to obtain GOS, which further were acylated with thionyl chloride to give acyl chloride bound GOS. Gold nanoparticles (AuNPs) were functionalized using 4-aminothiophenol in a single-phase system to introduce amino groups on their surface through the well-developed Au-S chemistry. Subsequently, amino groups of AuNPs were reacted with acyl chloride groups of GOS to form a novel hybrid material containing GOS and AuNPs. Fourier transform infrared spectroscopy (FT-IR), X-ray diffraction (XRD), energy dispersive X-ray (EDX) spectroscopy, ultraviolet – visible (UV-vis) spectroscopy were used to study the changes in surface functionalities and demonstrate the successful immobilization of AuNPs on GOS surface. High resolution transmission electron microscopy (HR-TEM) and field emission scanning electronic microscopy (FE-SEM) were employed to investigate the morphologies of prepared AuNPs and their distribution onto the GOS surface. Thermogravimetric analysis (TGA) was used to characterize the thermal stability of the samples on heating.

*This work was published in **Applied Surface Science, 2011, 257, 3350-3357.**

4.1. Introduction

The recent increase of interest in carbon family materials has opened new ways for producing arrays of novel functional nanomaterials. Among them, graphene, a two-dimensional material is composed of several planar sheets of sp^2-bonded carbon atoms, has attracted tremendous attention from scientific communities due to its unique thermal, chemical, physical, mechanical and electrical properties [1-5] and inexpensive source (graphite). Since it was discovered in 2004, graphene has been emerging as a promising candidate for generating novel hybrid materials with their excellent properties for a wide variety of potential applications in catalyst support [6, 7], electronic components [8, 9], chemical sensor [10, 11], Li ion batteries [12-14]. Among known strategies for preparation of the graphene-based hybrid materials, the chemical transformation of pristine graphite to graphite oxide (GO), which can be easily exfoliated in aqueous media to yield stable dispersions of mostly single-layer sheets of GOS is the most versatile and effective method. Furthermore, the presence of covalently attached oxygen containing groups, including hydroxyl, epoxy groups on the basal plane and carboxylic groups at the edge of GOS surface provides a handle for the chemical modification of graphene using well-developed carbon surface chemistry. Hence, GOS is often used as the starting nanoscale building block for developing graphene-based hybrid materials.

Similar to the early days of carbon nanotubes (CNTs) research, recently, a novel class of carbon-based functional nanomaterials has been developed to optimize the electrical, optical, biological, and catalyst properties via the combination of graphene with metal nanoparticles. As a novel carbon material, graphene is highly expected as a cheap substitute for CNTs to provide a cost-effective platform for developing hybrid materials

containing graphene and metal nanoparticles because it possesses large interfacial surface area far much better than its analogous counterpart, CNTs [15]. Hence, it is believed that the dispersion of metal nanoparticles on graphene sheets opens new ways for researchers in designing hybrid materials for various potential applications.

Among noble nanoparticles, AuNPs are one of the most studied nanomaterials, due to their remarkable properties [16-18]. It is well known that a number of studies have been made into the preparation of hybrid materials containing CNTs and AuNPs through the various functionalization strategies with potential applications in many fields such as catalyst, electronics, and biology [19-25]. However, up to now, only a few studies have been reported on the immobilization of AuNPs onto the surface of GOS for such applications. For example, Hong *et al* [26] have prepared AuNPs/graphene composites with controlled weight contents through self-assembling of AuNPs on 1-pyrene butyric acid functionalized graphene sheets under driving force of electrostatic interaction. Their composite exhibited highly sensitive and stable responses to uric acid. More recently, Li *et al* [27] reported on the preparation of AuNPs decorated graphene sheets in a facile route by reducing chloroauric acid in the presence of sodium dodecyl sulfate. According to their results, the graphene-AuNPs hybrid displayed impressive catalyst activity for Suzuki reaction. However, while they have obtained some achievements for potential applications, there is still one drawback, must be addressed to meet requirements for practical application. The drawback is that AuNPs may easily leach out from graphene sheets during application because the interactions between GOS and AuNPs are weak interactions. Therefore, an effective approach to solve this practical challenge is essential for generating graphene-based hybrid

materials.

Up to now, there have been no reports available on the immobilization of AuNPs on GOS surface by covalent bonding, which offers an effective way to overcome the problem mentioned above. In this study, we developed a new route for the preparation of novel hybrid nanomaterials through a simple amidation reaction. The three-step process includes: (1) AuNPs were modified using 4-aminothiophenol to introduce amino groups on their surface, (2) GOS was prepared by oxidizing graphite followed by exfoliation in ultrasonication bath, which further was acylated with thionyl chloride to give acyl chloride bound to GOS, (3) The immobilization of AuNPs on GOS surface was carried out by an amidation reaction between amino groups located on AuNPs surface and acyl chloride groups bound to GOS surface.

4.2. Experimental

4.2.1. Materials

Graphite powder from Sigma – Aldrich was used to prepare GO. 4-aminothiophenol (4-ATP), hydrogen tetrachloroaurate gold (gold solution; 30 wt.% in dilute HCl), sodium borohydride were purchased from Sigma – Aldrich and used as received. Tetrahydrofuran (Junsei, Japan) and thionyl chloride (Duksan Pure Chemical, South Korea) were distilled prior to use.

4.2.2. Synthesis of 4-aminothiophenol – functionalized AuNPs (4-ATP-*f*-AuNPs)

4-ATP-*f*-AuNPs were prepared by a modification of Brust method carried out in a single-phase system [28]. $HAuCl_4$ (0.3 mL) and 4-ATP (0.4 g) were dissolved in methanol (80 mL). Then, freshly prepared 0.4 mol dm^{-3} aqueous borohydride solution (12 mL) was added carefully in small portions

of *ca*. 1 mL with vigorous stirring. The solution mixture turned brown immediately, indicating the formation of gold nanoparticles. After continuous stirring 12 h at room temperature, the solvent was removed by distillation under decreased pressure without exceeding the temperature 45 ^{o}C. The dark residue was washed thoroughly with diethyl ether to remove excess 4-aminothiophenol. Then, the materials were washed with distilled water and dried under vacuum oven at 45 ^{o}C for 24 h to obtain the pure product as a dark-brown solid of 4-ATP-*f*-AuNPs.

4.2.3. Preparation of GOS

In a typical synthetic process, natural graphite powder (2.0 g) was added to cooled (0 ^{o}C) H_2SO_4 (300 mL). Then, $KMnO_4$ (20 g) and $NaNO_3$ (3 g) were added gradually while stirring. The mixture was then transferred to a water bath (30 ^{o}C) and stirred for 20 min. Deionized water (250 mL) was slowly added and the temperature was increased to 98 ^{o}C. The mixture was maintained at that temperature for 30 min. The reaction was terminated by adding deionized water (500 mL) followed by adding H_2O_2 solution (40 mL, 30%). The color of the mixture was changed to brilliant yellow, indicating the oxidation of pristine graphite to GO. Then, the mixture was filtered and washed with diluted HCl to remove metal ions. Finally, the product was washed repeatedly with distilled water until the pH became 7. The sample of GO was obtained after drying. To prepare GOS, the as-obtained GO was re-dispersed in distilled water to create a yellow-brown dispersion, and the exfoliation of GO to generate GOS was achieved by ultrasonication for 30 min. The resultant aqueous dispersion of brown GOS was stable [29].

4.2.4. Immobilization of AuNPs on the surface of GOS (AuNPs-*i*-GOS)

GOS (100 mg) was stirred with an excess amount of thionyl chloride

(40 mL) under nitrogen atmosphere at 80 ^{o}C for 24 h to yield acyl chloride bound GOS (GOS-COCl). Excess of $SOCl_2$ was removed by distillation under decreased pressure. After cooling down to the room temperature, the solid was suspended immediately in distilled THF (50 mL). Then, 4-ATP-*f*-AuNPs (6 mg) were added to the solution while stirring under nitrogen atmosphere at room temperature. The reactive –COCl groups of GOS-COCl reacted with the $–NH_2$ groups of the 4-ATP-*f*-AuNPs to form amide bonds. After continuous stirring 12 h, the solid was separated using filter membrane system and then, washed with ethanol and acetone. The product was dried in the vacuum oven at 40 ^{o}C.

4.2.5. Characterization techniques

HR-TEM images were recorded using Joel JEM 2010 instrument (Japan) with an accelerating voltage of 200 KV to observe the nanoscale structures, by placing a drop of the samples dispersed in ethanol on copper grids and drying. The morphology and elemental analysis of the hybrids were carried out by using FE-SEM images equipped with an EDX spectrometer (Hitachi JEOL-JSM-6700F system, Japan). The changes in the surface chemical bondings were recorded on FT-IR instrument (Perkin-Elmer Spectroscopy GX, USA), in the frequency range of 500 – 4000 cm^{-1}. The crystallographic states of the samples were determined by a Philips X'pert-MPD system diffractometer (Netherland) with Cu *Kα* radiation. Thermal studies of the materials were carried out on a Perkin-Elmer (USA) Pyris 1 analyzer. Before the test, all samples were carefully grinded to fine powder form. The samples were scanned within the temperature range from 50 to 700 ^{o}C at a heating rate of 10 ^{o}C min^{-1} under continuous nitrogen flow. The absorption spectra of the samples were obtained using a Perkin Elmer

Lambda 40 ultraviolet visible (UV – Vis) spectroscopy.

4.3. Results and discussion

4.3.1. Characterization of 4-ATP-*f*-AuNPs

The morphology, size distribution, surface structure, and bonding nature of 4-ATP-*f*-AuNPs were characterized using HR-TEM, XRD and FT-IR techniques. Fig. 1a shows the XRD pattern of the sample, which indicates the crystalline structure of 4-ATP-*f*-AuNPs. As labeled in Fig. 1a, the peaks at 38.21^{o}, 44.33^{o}, 64.58^{o}, 75.25^{o} are assigned to face-centered cubic *(fcc)* bulk gold of (111), (200), (220), (311), respectively. It is interesting to note that the peak corresponding to the (111) plane is more intense than other planes, indicating that the (111) plane is the predominant orientation, which is in good agreement with previous work [30]. On the other hand, Fig. 1b shows FT-IR spectrum of 4-ATP-*f*-AuNPs. As can be seen in Fig. 1b, the peaks at 3530 and 3414 cm^{-1} are attributed to stretching of the N-H band of primary amine groups of 4-ATP located on the AuNPs surface. Furthermore, the intense peaks at 1612 and 1490 cm^{-1} are assigned to stretching vibration of the C=C stretching of aromatic ring while peak at 936 cm^{-1} is associated with and C-N bond of 4-ATP bound to AuNPs surface.

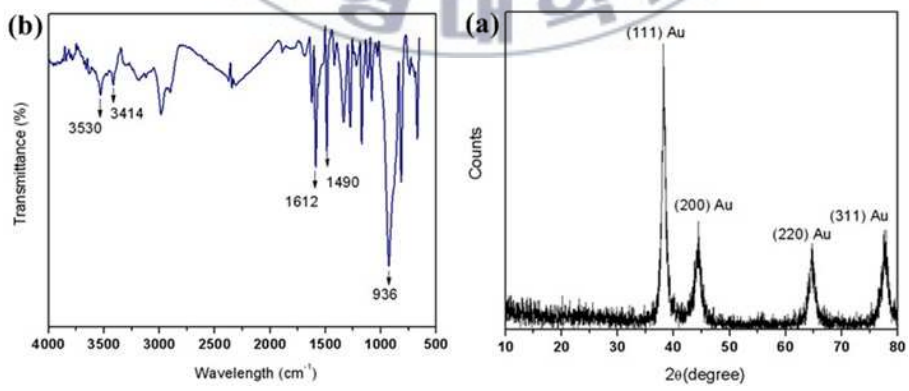

Figure 1. (a) XRD pattern and (b) FT-IR spectrum of 4-ATP-*f*-AuNPs.

In order to obtain chemical composition of the 4-ATP-*f*-AuNPs, EDX analysis was performed (Fig. 2). The spectrum details the presence of gold, sulfur, nitrogen, and carbon in the sample. These results clearly suggest that AuNPs were successfully functionalized by 4-ATP through the well-developed Au-S chemistry.

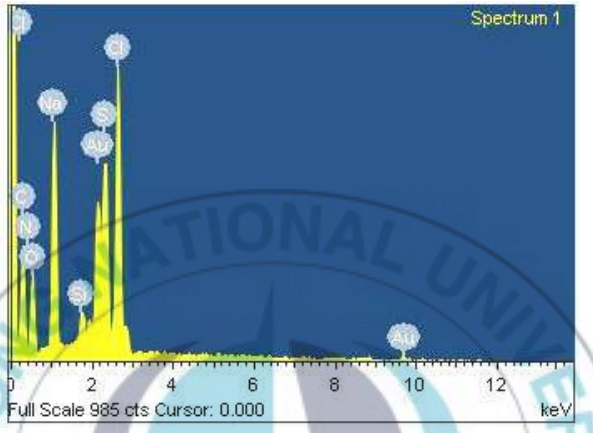

Figure 2. EDX spectrum of 4-ATP-*f*-AuNPs.

To understand the morphologies and size distribution of 4-ATP-*f*-AuNPs, the sample was imaged using HR-TEM technique as shown in Fig. 3. The TEM images of the sample show that 4-ATP-*f*-AuNPs are roughly spherical in shape with an average diameter of around 5 nm as shown in Fig 3(a-c). Furthermore, the size distribution of the 4-ATP-*f*-AuNPs was also studied and the result was shown in Fig. 3d.

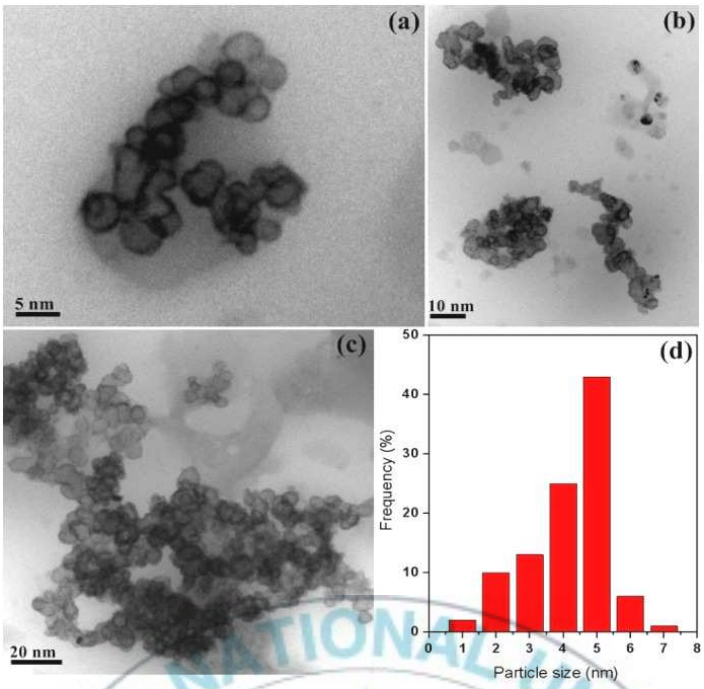

Figure 3. HR-TEM images (a-c) at different magnifications and size distribution (d) of 4-ATP-*f*-AuNPs.

4.3.2. Characterization of AuNPs-*i*-GOS hybrid material

The synthetic route for covalent immobilization of 4-ATP-*f*-AuNPS onto the GOS surface to obtain novel hybrid material is illustrated in Scheme 1. The characterization of the hybrid material was investigated using various techniques, including FT-IR, TGA, XRD, EDX and UV-vis spectroscopy. Fig. 4 shows FT-IR spectra of pristine graphite, GO, AuNPs-*i*-GOS hybrid, which obtained at different processing step. In the spectrum of pristine graphite, the peaks at 3005 and 1509 cm^{-1} are characteristic band of C-H and C=C stretching of aromatic ring. In the spectrum of GO, the presence of carboxylic groups after oxidation step was confirmed with intense peak at 1721 cm^{-1} and weak peak at 1253 cm^{-1}, which correspond to the stretching of C=O bond and C-O bond, respectively. Additionally, the broad band at 3141 cm^{-1} and sharp peak at 1501 cm^{-1} could be assigned to stretching of OH groups on the GO surface and C=C stretching of aromatic

ring in the sample, respectively. The FT-IR spectrum of AuNPs-*i*-GOS differs from that of GO as evidenced by the presence of new peaks at 3452 and 1612 cm^{-1}, whereas the old peaks at 3141 and 1721 cm^{-1} almost disappears. It can be clearly seen in Fig. 4c, the new peaks emerges at 3452 and 1612 cm^{-1} are assigned to N-H stretching and C=O stretching of amide groups on the GOS surface, respectively. The characteristic band of C-H and C=C stretching of aromatic ring was still observed at 3008 and 1492 cm^{-1}. These results clearly indicate that 4-ATP-*f*-AuNPs were well immobilized on the GOS surface via amide linkages.

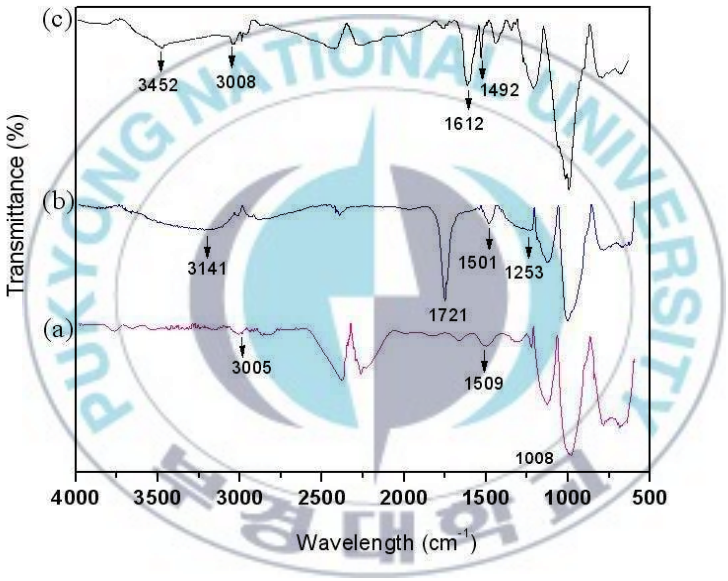

Figure 4. FT-IR spectra of (a) pristine graphite, (b) GO, and (c) AuNPs-*i*-GOS.

XRD is an effective method to study the interlayer changes of graphite related powders of prepared materials. Fig. 5 shows the XRD patterns of pristine graphite, GO and AuNPs-*i*-GOS. While the intense peak appears at $2\theta = 26.6^{o}$ (Fig. 5a), corresponding to the (002) plane of pristine graphite,

the GO pattern shows a characteristic peak at $2\theta = 11.7^{o}$ (Fig. 5b), indicating the presence of oxygen containing functional groups after the liquid-phase oxidation. Because the groups cause the GO sheets to stack more loosely, the d-spacing of GO layers (0.43 nm) is larger than that of the layers of pristine graphite (0.25 nm) [31]. As to the AuNPs-*i*-GOS, except the weak peak at $2\theta = 22.2^{o}$ corresponding to the (002) plane of GOS, all other diffraction peaks appear at $2\theta = 38.34^{o}$, 44.59^{o}, 64.76^{o}, 77.65^{o} can be unambiguously indexed to *fcc* bulk gold (Fig. 5c), which are in good agreement with the standard values in the standard card of gold (JCPDS 04-784). These results further confirm that AuNPs were successfully immobilized on the GOS surface.

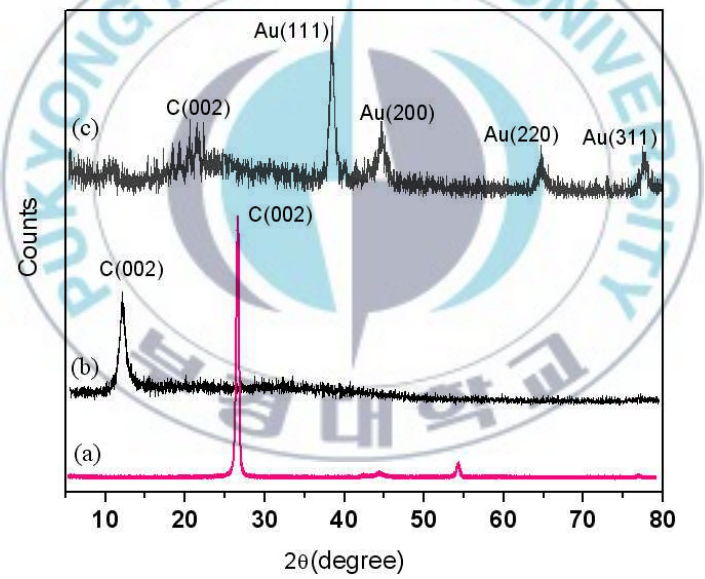

Figure 5. XRD patterns of (a) pristine graphite, (b) GO, and (c) AuNPs-*i*-GOS.

In order to understand the chemical composition of the prepared hybrid material, EDX spectra of GO and AuNPs-*i*-GOS were recorded as shown in Fig. 6. While EDX spectrum of GO shows that the sample only

contains oxygen and carbon elements (Fig. 6a), the EDX spectrum of AuNPs-*i*-GO sample indicates the presence of AuNPs on the GOS surface after covalent functionalization (Fig. 6b).

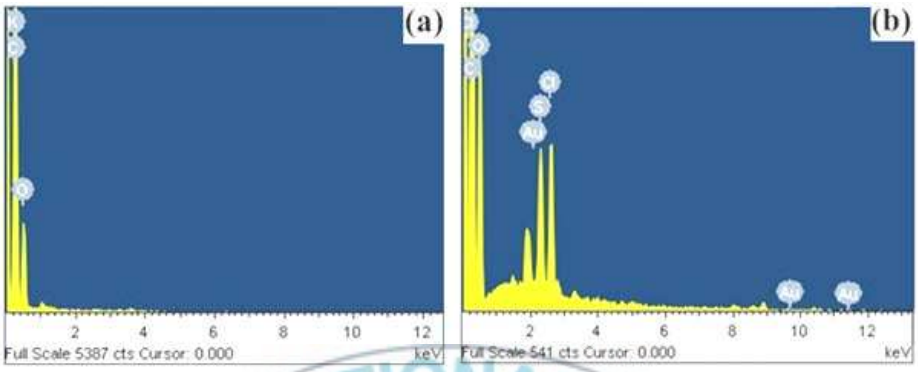

Figure 6. EDX spectra of (a) GO and (b) AuNPs-*i*-GOS.

Fig. 7 shows UV-vis absorption spectra of prepared hybrid material, together with those of GO, 4-ATP-*f*-AuNPs and naked AuNPs for comparison. As can be seen in Fig. 7a, the spectrum of GO showed a weak shoulder at around 230 nm, corresponding to $\pi \rightarrow \pi^*$ transitions of aromatic C=C bonds and a characteristic absorption at around 260 nm, which can be attributed to $n \rightarrow \pi^*$ transitions of C=O bonds [32]. In the case of 4-ATP-*f*-AuNPs sample, the spectrum shows a surface plasmon absorption band at 560 nm (Fig. 7b). For the naked AuNPs used in the present work with a diameter of about 5 nm, typical surface plasmon band is around 525 nm as shown in inset graph. It is interesting to note that the surface plasmon resonance band of 4-ATP-*f*-AuNPs displays a red-shift and broadens in comparison with that of naked AuNPs due to the interaction between 4-ATP ligand and the electron cloud on the surface of the gold, which is consistent with previous reports [33, 34]. As to AuNPs-*i*-GOS sample, the

characteristic absorption band at around 260 nm was still observed with the relative decrease in the intensity in comparison with that of GO, while the surface plasmon band of AuNPs appeared at 560 nm as a weak and broad band (Fig. 7c). These results strongly suggest that AuNPs were well bound onto GOS surface.

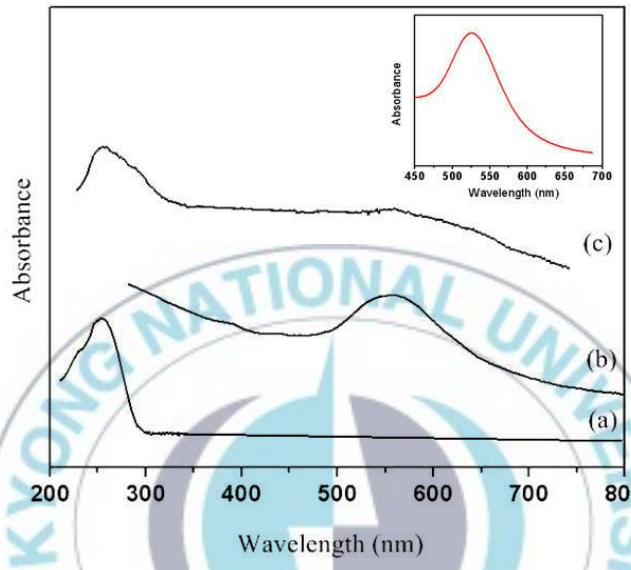

Figure 7. UV-vis spectra of (a) GO, (b) 4-ATP-*f*-AuNPs and (c) AuNPs-*i*-GOS. The inset graph shows absorption spectrum of naked AuNPs (~5 nm in diameter).

4.3.3. Thermal stability of hybrid material

In order to investigate the thermal behavior and stability of the samples after modification, TGA were conducted as shown in Fig. 8. TGA trace of pristine graphite shows little weight loss, which is about 2% of its total weight below 700^{o}C due to the removal of physically adsorbed water. In comparison with pristine graphite, GO shows much lower thermal stability. Although GO also starts to lose weight upon heating below 100^{o}C, the main weight loss takes place around 180^{o}C and lose up to 98% of its

total weight, presumably due to pyrolysis of the labile oxygen containing functional groups present in the material, yielding CO, CO_2 and steam [35]. Comparing with GO, the thermal stability of AuNPs-*i*-GOS hybrid is higher than that of GO. It can be clearly seen in Fig. 8c. TGA traces of AuNPs-*i*-GOS shows a gradual weight loss in the entire temperature range, which is about 37% of its total weight. This well suggests that the thermal stability of prepared hybrid material was better improved due to the binding of AuNPs to the GOS surface through the covalent functionalization.

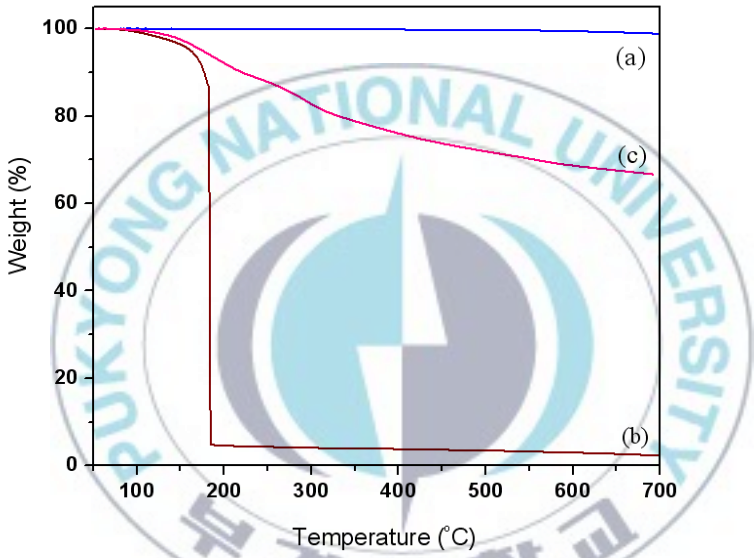

Figure 8. TGA curves of (a) pristine graphite, (b) GO, and (c) AuNPs-*i*-GOS.

4.3.4. Morphologies of hybrid material

The morphologies of GO and AuNPs-*i*-GOS hybrid were studied using HR-TEM technique. Fig. 9 shows the HR-TEM images of the samples at different magnifications. As shown in Fig. 9a and 9b, the presence of a mixture of GO layers was observed. Most of the layers are bilayer or few layers of graphene are present (marked by arrows). They are rippled and

entangled with each other like a silk weave form due to extremely small thickness of the GOS, suggesting a flexible structure of the graphene sheets. The direct evidence for the successful immobilization of AuNPs onto the GOS surface was given by HR-TEM images in Fig. 9c and 9d. It can be clearly seen that AuNPs with diameter of about 5nm were homogeneously immobilized along with GOS surface. Furthermore, no free AuNPs were observed outside of GOS surface, indicating the AuNPs were well bound to GOS surface via strong covalent bonding of amide linkages. It is interesting to note that the density of AuNPs at the edges of GO are relatively higher than that on the basal plane of GOS (Fig. 9c). It could be explained by higher density of acyl chloride functional groups on these regions.

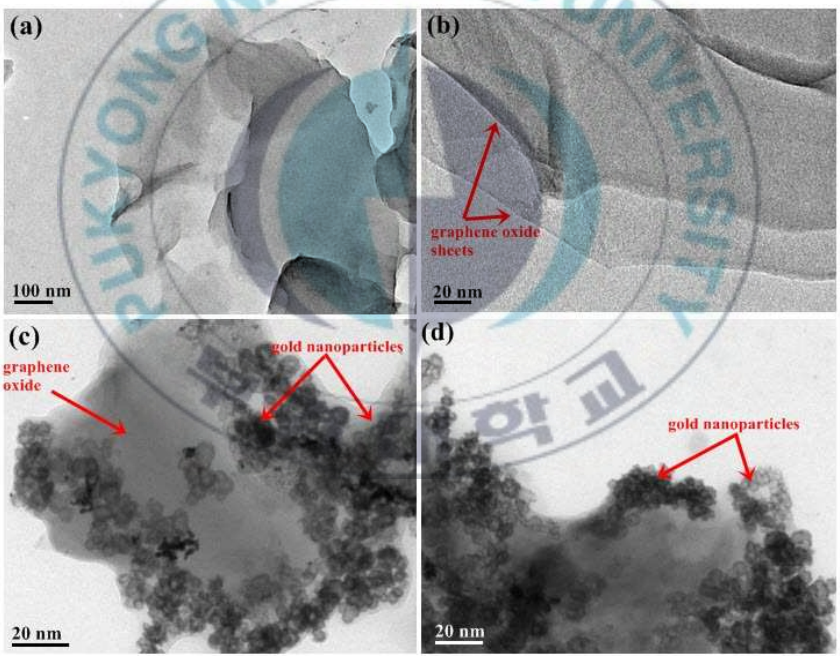

Figure 9. TEM images of GOS (a, b) and AuNPs-*i*-GOS (c, d).

In order to further investigate the surface morphology of the prepared hybrid material and the dispersion of AuNPs on the GOS surface,

AFM images were recorded. As can be seen in Fig. 10a and 10b, the bright regions are related to the AuNPs, which were immobilized on the GOS surface after amidation reaction. On the other hand, the section analysis of the image shows a background height of 1 – 3nm which corresponds to the GOS thickness. Furthermore, the peaks seen in this section analysis correspond to the AuNPs immobilized on the GOS surface. It was interesting to note that these peaks are different in height although HR-TEM images confirm our ability to achieve uniform distribution of the AuNPs with size of 5nm on the GOS surface. The reason for this could be that the AuNPs were immobilized on rough surfaces of graphene sheets on the mica substrate.

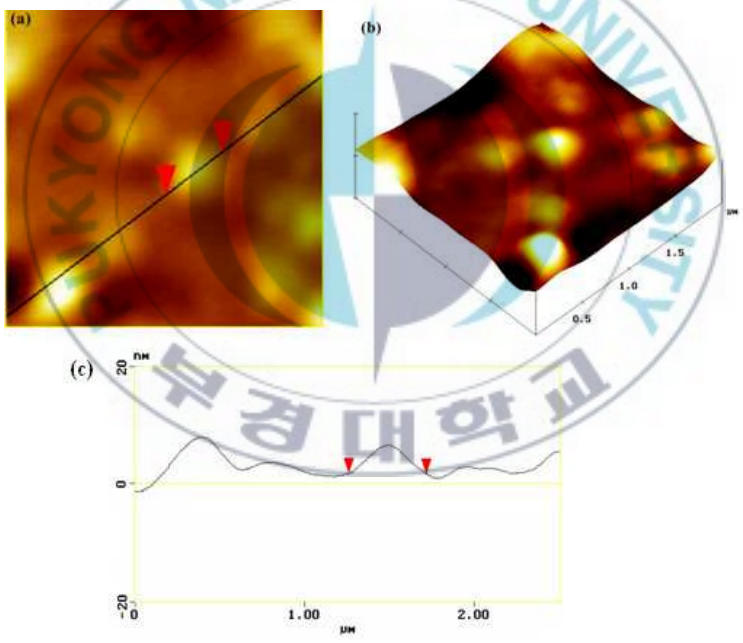

Figure 10. (a) AFM image, (b) 3D image and (c) section analysis image of AuNPs-*i*-GOS hybrid.

Conclusions

In conclusion, AuNPs-*i*-GOS hybrid nanomaterial has been successfully prepared by a simple amidation reaction. Since the weak interactions between nanoparticles and GOS surface were replaced by strong covalent bonds, the surface functionalized AuNPs with a diameter of about 5 nm were well immobilized onto the surface of GOS, which guarantees efficient properties of prepared hybrid for various potential applications. We believe that the simple preparation method of AuNPs-*i*-GOS hybrid in present study is particularly promising for the design of novel functional nanomaterials. Considering the unique properties of AuNPs and inexpensive source of GOS, in the near future, these hybrid materials are expected to provide a cost-effective platform for potential applications in various fields, including nanodevices, nanoelectronics, nanobiotechnology and heterogeneous catalysts.

Bibliography

1. S. Park, K.S. Lee, G. Bozoklu, W. Cai, S.T. Nguyen, R.S. Ruoff, ACS Nano 3 (2008) 572.
2. J. Wu, W. Pisula, K. Müllen, Chem. Rev. 107 (2007) 718.
3. M.J. Allen, V.C. Tung and R.B. Kaner, Chem. Rev. 110 (2010) 132.
4. C.G. Navarro, M. Burghard, K. Kern, Nano Lett. 8 (2008) 2045.
5. C.G. Navarro, R.T. Weitz, A.M. Bittner, M. Scolari, A. Mews, M. Burghard, and K. Kern, Nano Lett. 7 (2007) 3499.
6. R. Kou, Y. Shao, D. Wang, M.H. Engelhard, J.H. Kwak, J. Wang, V.V. Viswanathan, C. Wang, Y. Lin, Y. Wang, I.A. Aksay, J. Liu, Electrochem. Commun. 11 (2009) 954.

7. Y. Li, X. Fan, J. Qi, J. Ji, S. Wang, G. Zhang, and F. Zhang, Nano Res. 3 (2010) 429.
8. X. Wang, L. Zhi, K. Müllen, Nano Lett. 8 (2008) 323.
9. V.Y. Aristov, G. Urbanik, K. Kummber, D.V. Vyalikh, O.V. Molodtsova, A.B. Preobrajenski, A.A. Zakharov, C. Hess, T. Hänke, B. Büchner, I. Vobornik, J. Fujii, G. Panaccione, Y.A. Ossipyan, M. Knupfer, Nano Lett. 10 (2010) 992.
10. J.D. Fowler, M.J. Allen, W.C. Tung, Y. Yang, R.B. Kaner, and B.H. Weiller, ACS Nano 3 (2009) 301.
11. X. Kang, J. Wang, H. Wu, I.A. Aksay, J. Liu, Y. Lin, Biosens. Bioelectron. 25 (2009) 901.
12. G. Wang, X. Shen, J. Yao, J. Park, Carbon 47 (2009) 2049-2053.
13. J.K. Lee, K.B. Smith, C.M. Hayner, and H.H. Kung, Chem. Commun. 46 (2010) 2025.
14. D. Choi, D. Wang, V.V. Viswanathan, I.T. Bae, W. Wang, Z. Nie, J.G. Zhang, G.L. Graff, J. Liu, Z. Yang, T. Duong, Electrochem. Commun. 12 (2010) 378.
15. S. Stankovich, D.A. Dikin, G.H.B. Dommett, K.M. Kohlhaas, E.J. Zimney, E.A. Stach, R.D. Piner, S.T. Nguyen and R.S. Ruoff, Nature 442 (2006) 282.
16. Z. Zhong, S. Patskovskyy, P. Bouvrette, J.H.T. Luong and A. Gedanken, J. Phys. Chem. B 108 (2004) 4046.
17. J. Zhou, J. Ralston, R. Sedev, D.A. Beattie, J. Colloid Interface Sci. 331 (2009) 251.
18. J. Han, Y. Liu, and R. Guo, J. Am. Chem. Soc. 131 (2009) 2060.
19. T.A. Pham, S.M. Son, Y.T. Jeong, Synth. React. Inorg. Met. – Org. Chem. 40 (2010) 216.

20. D. Gingery, P. Bühlmann, Carbon 46 (2008) 1966.
21. A. Tello, G. Cardenas, P. Häberle, R.A. Segura, Carbon 46 (2008) 884.
22. S.Y. Moon, T. Kusunose, S. Tanaka, T. Sekino, Carbon 47 (2009) 2924.
23. R. Zanella, E.V. Basiuk, P. Santiago, V.A. Basiuk, E. Mireles, I.P. Lee, and J.M. Saniger, J. Phys. Chem. B 109 (2005) 16290.
24. A. Velamakanni, C.W. Magnuson, K.J. Ganesh, Y. Zhu, J. An, P.J. Ferreira, and R.S. Ruoff, ACS Nano 4 (2010) 540.
25. T.G. Kim, D. Ragupathy, A.I. Gopalan, and K.P. Lee, Nanotechnology 21 (2010) 134021.
26. W. Hong, H. Bai, Y. Xu, Z. Yao, Z. Gu, and G. Shi, J. Phys. Chem. C 114 (2010) 1822.
27. Y. Li, X. Fan, J. Qi, J. Ji, S. Wang, G. Zhang, F. Zhang, Mater. Res. Bull. 45 (2010) 1413.
28. M. Brust, J. Fink, D. Bethell, J. Schiffrin and C. Kiely, J. Chem. Soc. Chem. Commun. (1995) 1655.
29. T.A. Pham, N.A. Kumar, Y.T. Jeong, Synth. Met. 160 (2010) 2028.
30. P. Kannan, and S.A. John, Nanotechnology 19 (2008) 085602.
31. M. Fang, K. Wang, H. Lu, Y. Yang, S. Nutt, J. Mater. Chem. 112 (2009) 7098.
32. X. Zhao, Q. Zhang, and D. Chen, Macromolecules 43 (2010) 2357.
33. M. Geng, Y. Zhang, Q. Huang, B. Zhang, Q. Li, W. Li, J. Li, Carbon 48 (2010) 3570.
34. J. Hu, J. Shi, S. Li, Y. Qin, Z.X. Guo, Y. Song, D. Zhu, Chem. Phys. Lett. 401 (2005) 352.
35. S. Stankovich, D.A. Dikin, R.D. Piner, K.A. Kohlhaas, A. Kleinhamma, Y. Jia, Y. Wu, S.T. Nguyen, R.S. Ruoff, Carbon 45 (2007) 1558.

Summary and Outlook

This thesis has been focused on the preparation of graphene/nanoparticles hybrid nanostructures using new and simple strategies by the way of chemical covalent functionalizations. We have successfully immobilized different types of functional nanoparticles on graphene oxide surface, including gold nanoparticles, magnetic nanoparticles and CdS quantum dots. The characterization and properties of the prepared hybrid has been investigated in detail using various analytical techniques. The merit of this work is that functionalized nanoparticles were strong bound to graphene surface by covalent bonding which prevents nanoparticles leach out from graphene surface during practical applications. Considering the importance of these nanoparticles as well as unique properties of graphene and its inexpensive source, in the future, these hybrid materials could be useful as a cost-effective platform for potential applications.

List of Publications

The following publications present the results obtained in the framework of this Masters duration.

[1] **T.A. Pham,** J.S. Kim, D. Kim and Y.T. Jeong, Facile preparation of water dispersible graphene nanosheets by covalent functionalization with poly (m-aminobenzene sulfonic acid), *submitted to Polymer Science and Engineering, 2011*.

[2] **T.A. Pham**, J.S. Kim, J.S. Kim, Y.T. Jeong, One step reduction of graphene oxide by L-glutathione. Colloids and Surfaces A: Physicochemical and Engineering Aspects, **384** (2011) 543.

[3] **T.A. Pham.** J.S. Kim, B.K. Cho, S.M. Son, Y.T. Jeong "Facile preparation of water dispersible adenosine-functionalized graphene nanosheets" Synth. React. Inorg. Met. Org. Chem *(accepted, 2011)*.

[4] **T.A. Pham**, B.C. Choi, K.T. Lim, Y.T. Jeong, "*A simple approach for immobilization of gold nanoparticles on graphene oxide sheets by covalent bonding*", Applied Surface Science **257** (2011) 3350-3357.

[5] **T.A. Pham**, B.C. Choi, Y.T. Jeong, "*Facile covalent immobilization of cadmium sulfide quantum dots on graphene oxide nanosheets: Preparation, characterization, and optical properties*", Nanotechnology, **21** (2010) 465603.

[6] **T.A. Pham,** K.T. Lim, and Y.T. Jeong, "*Water dispersability of gluconate functionalized multi-walled carbon nanotubes and facile strategy for construction of hybrid nanostructure*", Materials technology: Advanced Performance Materials *(accepted, 2010)*.

[7] **T.A. Pham**, N.A. Kumar, and Y.T. Jeong, "*Facile Preparation of Boronic acid Functionalized Fe-core/Au-shell Magnetic Nanoparticles for Covalent Immobilization of Adenosine*", Colloids and Surfaces A: Physicochemical and Engineering Aspects, **370** (2010) 95.

[8] **T.A. Pham**, N.A. Kumar, and Y.T. Jeong, "*Covalent functionalization of graphene nanosheets with polyglycerol and their use as templates for anchoring magnetic nanoparticles*", Synthetic metal, **160** (2010) 2028.

[9] **T.A. Pham,** S.M. Son, and Y.T. Jeong, "*Water-Dispersible Multi-Walled Carbon Nanotubes and Novel Hybrid Nanostructures*" Synth. React. Inorg. Met.-Org. Chem., **40** (2010) 216.